




## Article

# Dynamic Stability Evaluation of an Integrated Biodiesel-Geothermal Power Plant-Based Power System with Spotted Hyena Optimized Cascade Controller

Arindita Saha <sup>1</sup>, Puja Dash <sup>2</sup> , Naladi Ram Babu <sup>3</sup>, Tirumalasetty Chiranjeevi <sup>4</sup> , Mudadla Dhananjaya <sup>5</sup> and Łukasz Knypinski <sup>6,\*</sup> 

<sup>1</sup> Department of Electrical Engineering, Regent Education & Research Foundation Group of Institutions, Kolkata 700121, West Bengal, India

<sup>2</sup> Department of Electrical and Electronics Engineering, Gayatri Vidya Parishad College of Engineering (Autonomous), Visakhapatnam 530048, Andhra Pradesh, India

<sup>3</sup> Department of Electrical & Electronics Engineering, Aditya Engineering College, Surampalem 533437, Andhra Pradesh, India

<sup>4</sup> Department of Electrical Engineering, Rajkiya Engineering College Sonbhadra, Churk 231206, Uttar Pradesh, India

<sup>5</sup> Department of EEE, Anil Neerukonda Institute of Technology and Science (A), Visakhapatnam 531162, Andhra Pradesh, India

<sup>6</sup> Faculty of Automatic Control, Robotic and Electrical Engineering, Poznan University of Technology, 60-965 Poznan, Poland

\* Correspondence: lukasz.knypinski@put.poznan.pl



**Citation:** Saha, A.; Dash, P.; Babu, N.R.; Chiranjeevi, T.; Dhananjaya, M.; Knypinski, L. Dynamic Stability Evaluation of an Integrated Biodiesel-Geothermal Power Plant-Based Power System with Spotted Hyena Optimized Cascade Controller. *Sustainability* **2022**, *14*, 14842. <https://doi.org/10.3390/su142214842>

Academic Editors: Marek Jasinski, Zbigniew Leonowicz, Michał Jasiński and Elżbieta Jasińska

Received: 4 October 2022

Accepted: 7 November 2022

Published: 10 November 2022

**Publisher's Note:** MDPI stays neutral with regard to jurisdictional claims in published maps and institutional affiliations.



**Copyright:** © 2022 by the authors. Licensee MDPI, Basel, Switzerland. This article is an open access article distributed under the terms and conditions of the Creative Commons Attribution (CC BY) license (<https://creativecommons.org/licenses/by/4.0/>).

**Abstract:** The perception of automatic generation control (AGC) has a massive part in delivering eminence power in an interrelated structure. To acquire eminence power by monitoring the fluctuations of frequency and tie-link power, an appropriate controller strategy is essential. This work explores AGC learning under the traditional situation. In this study, we employ a cascade controller with proportional amalgamation with a tilt-integral-derivative with a filter (TIDN) and fractional order integral-derivative (FOID), named TIDN-FOID. In order to acquire the controller's attributes, a meta-heuristic optimization algorithm spotted hyena optimizer (SHO) is employed. Several investigations express the excellency of the TIDN-FOID controller over other controllers from outlook regarding the lessened level of peak\_overshoot, peak\_undershoot, and settling\_time for the considered structure. The structure comprises thermal, biodiesel units in area 1, thermal, and geothermal units in area-2, and hydrothermal units in area-3. Both biodiesel and GPP have a better effect on system dynamics even in the presence of time delay. Action in the redox flow battery is also examined, providing a noteworthy outcome. Eigenvalue assessment is carried out to comment on the stability of the system. TIDN-FOID parameter values at nominal conditions are appropriate for a higher disturbance value without the need for optimization.

**Keywords:** automatic generation control; geothermal power plant; redox flow battery; biodiesel plant; spotted hyena optimizer; particle swarm optimization; controller; time delay

## 1. Introduction

Proper coordination between the amounts of power generation and demand and losses is essential for better power system performance. This balance may be disrupted during periods of heavy load demand. If this balance is not maintained or observed at the right time, it may lead to huge damage by providing huge aberration in frequency and tie-line power from the base values. These disproportions were subdued by the conception of AGC [1–3]. Elgerd et al. [4] provided the basic mathematical formulation of AGC in the case of a two-area thermal system. In the past, works on AGC were mainly confined to a single area system [5–7]. Later, studies included two-area [8,9], three-area [9–11], four-area [12],

and five-area [13] systems with the inclusion of non-linearity, such as the generation rate constraint, and also sometimes the governor dead band. Most of the works used thermal as generating units. Nanda et al. [14] have performed an analysis for a system having hydrothermal sources. Abraham et al. [15] assessed a two-area hydrothermal system. Arya [16] considered the AGC system of varied generating sources, such as thermal power, hydropower and diesel. Panwar et al. [17] analyzed a hydropower-dominating system. Arya et al. [18] considered the AGC system of varied generating sources, such as thermal power, hydropower, and gas. Very few papers in the literature [19] reflected on the usage of non-linearity time delay along with other forms of non-linearity. The presence of time delay in a three-area hydrothermal system has not yet been discussed in the literature. Hence, it can be carried out for analysis.

Excessive use of one energy source for every purpose rigorously depletes resources. Overall, besides depletion, it also releases toxic gases which are hazardous to the environment. Thus, it is essential to combine conventional and renewable energy sources. The utmost communal forms of readily available inexhaustible bases are solar and wind energy. Numerous articles have described the contribution of solar and wind energy with respect to AGC knowledge, both in a sole arena and with unified arrangements. Moreover, geothermal and biodiesel energy sources have also been researched. Geothermal energy is a kind of thermal energy which is stored in the earth. Consequently, this category of energy can be extracted from the earth's shell. Biodiesel plants employ biodiesel to drive generators. Tasnin et al. [20] emphasized the practice of geothermal power plants (GPPT) in AGC learning along with conventional sources. Sharma et al. [21] analyzed a photovoltaic-incorporated thermal system. Biodiesel is formed from oil that has been pulled out from varied plants, such as sunflower, palm, or soybean. Most commonly, palm oil is used for biodiesel. Biodiesel is a type of renewable fuel. The authors in [22] reported the usage of biodiesel in the case of an isolated scheme. The combination of GPPT and biodiesel plants in AGC knowledge has not yet been replicated in literature. Thus, the hydrothermal system incorporated with GPPT and biodiesel in time delay calls for further extensive assessments.

In a unified scheme, the arrangement can be steadied with diminished alteration in glitches with the assistance of numerous energy storage devices (ESD), such as battery energy storage devices (BESDs) [23] and ultra-capacitors [24]. There are many types of BESDs, such as lead-acid, lithium-ion, sodium sulfur, metal-air, and redox flow batteries (RFBs). RFB can be employed when there is a need for large storage facilities. Among all these types of BESDs, in light of AGC, RFBs show much potential [25,26]. It has a lengthier running duration and enables great power capacity. Moreover, it even has guaranteed profits, such as swift slight-interval surplus capability, huge effectiveness, exposure from own-expulsion matters, low-priced, and not being cluttered up by unforeseen charging/discharging. As RFBs have so many advantages, their application in a hydrothermal-biodiesel-GPPT system with time delay needs elaborate assessments.

The proper selection of a secondary controller is of high importance in AGC learning regarding control. Numerous forms of subsidiary controllers, such as integer-order (InOr), fractional-order (FrOr), and cascade controllers (CaC), are stated in literature to be linked to AGC. The usage of various InOr controllers, such as integral (I) [26], proportional-integral (PI) [27], and proportional-integral-derivative with filter (PIDN) [28], is reflected in the literature. Two [29] or three [30] higher degrees of freedom controllers have been inspected in this ground of training, which were also of the InOr type. Limited FrOr controllers that have found to be of use are FOPI [31], FOPIDN [32–34], and proportional with TIDN [35–38]. The literature on AGC systems provides an argument about the training of InOr amalgamated controllers (PD-PID) [39], FrOr amalgamated controllers (FOPI-FOPD) [20], and the assemblage of InOr and FrOr controllers (PIDN-FOPD). Arya et al. [40] analyzed a system with a cascade  $\lambda D\mu N$  controller. In addition to all these controllers, various authors reported on fuzzy and intelligent controllers. Sharma et al. [41] worked on an AGC system incorporating ANN controllers. Sharma et al. [42] have reported on the usage of fuzzy PIDF controllers. However, the series cascade combination of TIDN with

FrOr integral-derivative termed TIDN-FOID has not yet been quantified in AGC works. Additionally, the function of the TIDN-FOID subsidiary controller in this trinity-arena hydrothermal-biodiesel-GPPt arrangement has not yet been researched.

The enactment of any subordinate controllers is dominant solitary if the finest values of attributes are suitably selected. These could be prepared with the aid of traditional/optimization practices [43–60]. However, the traditional practice has moderate difficulty to deliver suboptimum consequences. A few algorithms used for AGC are bacterial foraging optimization (BFO) [10], whale optimization algorithm (WOA) [19], sine-cosine algorithm (SCA) [20], cuckoo search (CS) [29], particle swarm optimization (PSO) [33], coyote optimizer algorithm (COA) [37], bat algorithm (BA) [39], salp swarm algorithm [50], grey wolf [51], firefly algorithm (FA) [53], flower pollination algorithm (FPA) [54], differential evolution (DE) [55], and Jaya algorithm [56]. A newly established bioinspired meta-heuristic procedure labeled as SHO has also been developed [57]. SHO was recognized from spotted hyenas' behavioral nature, which depicts the communal promise amidst spotted hyena and their cooperative performances. To a great wonder, SHO has not identified its implementation in AGC learning for obtaining premium values of controller attributes, thus demanding advance examination.

With concern to overhead deliberations, the major persistence of the current artifact is as follows:

- (a) Construction of a trio-arena structure with thermal-thermal-biodiesel energy in arena-1, thermal-thermal-GPPt energy in arena-2, and hydrothermal energy in arena-3.
- (b) The attributes of PIDN/TIDN/TIDN-FOID are concurrently augmented separately via the SHO algorithm so as to attain an outstanding controller.
- (c) The impact of biodiesel and GPPt energy on system dynamics is studied with the best obtained controller from (b).
- (d) The impact of time delay on system dynamics is studied with the best obtained controller from (b).
- (e) The impact of RFB on system dynamics is studied with the best obtained controller from (b).
- (f) Eigenvalue assessment is performed to comment on the stability of the system.
- (g) Sensitivity analysis is performed to examine the robustness of the best controller's gains with a higher value of step load disturbance.

### 1.1. Novelty of Work

In the view of above, the novelties of the article are as follows:

- (a) The performance evaluation of RFB-biodiesel-GPPt-based interconnected AGC system with time delay under conventional scenario are carried out for the first time;
- (b) To design a new cascade TIDN-FOID controller in AGC studies;
- (c) Application of RFB-based biodiesel and GPPt in AGC studies;
- (d) A maiden effort was made to conduct the stability analysis considering eigenvalue assessment and sensitivity analysis;
- (e) Solicitation of SHO algorithms for the instantaneous optimization of the suggested cascade controller.

### 1.2. Contribution

Thus, the main contributions of the article are as follows:

- (a) Investigations are carried out with RFB considering biodiesel and GPPt plants in conventional AGC systems;
- (b) A new cascade TIDN-FOID is proposed and its performance is found to be better than PIDN and TIDN controllers;
- (c) Controller parameters are optimized by the SHO algorithm and the system dynamics with SHO optimized TIDN-FOID enhances system dynamics over WOA, CS, FA, and PSO techniques;

- (d) Studies on the selection of performance indices are carried out, and it is observed that ISE outperforms ITSE, IAE, and ITAE;
- (e) System dynamics with RFB considering biodiesel and GPpT are found to be better than other combinations;
- (f) Case studies on various values of time delays are carried out, and it is evident that with time delay the system dynamics are degraded;
- (g) Sensitivity analysis is carried out, and it is suggested that the obtained controller parameters at nominal conditions are robust.

### 1.3. Organization of the Article

The entire article is divided into different sections. Section 1 provides an introduction, Section 2 includes details related to system, Section 3 describes the controller details, Section 4 details the spotted hyena optimizer, Section 5 discusses the results, and Section 6 involves the conclusion of the article, followed by an appendix and references.

## 2. Scheme Representation

### 2.1. Overall Representation of the Scheme

A trinity-arena structure of a non-identical kind is engaged with the interpretation of analyses with an arena size ratio of 2:3:4. The structure includes thermal, thermal, and biodiesel (T-T-Bd) resources as generating elements in arena-1. Similarly, thermal, thermal, and geothermal power plants (GPpT) (T-T-GPpT) energy is used in arena-2 and thermal and hydro (T-H) energy in arena-3. The traditional diesel plant is currently replaced with biodiesel elements, since they are not contaminated as well recyclable and of somewhat denser, lesser viscosity; furthermore, it results in a lower amount of carbon monoxide. Consequently, it can be employed as a reserve for a power source. It entails a combustion engine and valve controller. The primary order transfer function (Trfn) of the valve controller and ignition appliance of biodiesel element is specified by Equations (1) and (2), respectively [22]:

$$Tf_{valve\ regulator_{Bio-diesel}} = \frac{K_{VR}}{1 + sT_{VR}} \quad (1)$$

$$Tf_{Combustion\ engine_{Bio-diesel}} = \frac{K_{CE}}{1 + sT_{CE}} \quad (2)$$

Geothermal energy is a possible inexhaustible source of energy where underground thermal energy is transmuted into electrical energy. The Trfn modeling of GPpT is comparable to thermal elements but it does not have the cistern for warming condensation. The initial order Trfn of the governor and turbine of GPpT are specified by Equations (3) and (4), respectively [20]:

$$Tf_{G_{GPP}} = \frac{1}{1 + sG_{GPP}} \quad (3)$$

$$Tf_{T_{GPP}} = \frac{1}{1 + sT_{GPP}} \quad (4)$$

where  $G_{GPP}$  and  $T_{GPP}$  are the time constants of the governor and turbine of GPpT, respectively. These standards are attained by augmentation procedure SHO, given the restrictions.

The systems that are associated with a generation rate constraint and governor dead band display non-linearity. The contributing factors ( $cf$ ) of every generating unit of individual arenas are  $cf_{11} = 0.4$ ,  $cf_{12} = 0.4$ , and  $cf_{13} = 0.2$  in arena-1,  $cf_{21} = 0.4$ ,  $cf_{22} = 0.39$ , and  $cf_{23} = 0.21$  in arena-2, and  $cf_{31} = 0.655$  and  $cf_{32} = 0.345$  in arena-3. This makes up structure-1. The system with only thermal energy in area-1 and 2 and thermal and hydro energy in area-3 is considered structure-2. Consequently, structure-1 is integrated with time delay in all areas in order to make the system more practical. This is treated as scheme-3. The energy storage section, specifically RFB, is included in area-1. This is treated as structure-4. The representation and Trfn prototypical of schemes are shown in Figure 1. The basic standards of the scheme constraints are specified in Appendix A. The finest standards of controller

attributes are attained by the assistance of spotted hyena optimizer procedure using the integral squared error as the performance index ( $PI_{ISE}$ ) specified by Equation (5) [19]:

$$PI_{ISE} = \int_0^T \{ (\Delta f_1)^2 + (\Delta f_2)^2 + (\Delta f_3)^2 + (\Delta P_{tie_{1-2}})^2 + (\Delta P_{tie_{2-3}})^2 + (\Delta P_{tie_{1-3}})^2 \} dt \quad (5)$$

### 2.2. Energy Stowing Device-RFB

RFB is a category of flow batteries, established on the base of immobile energy stowage practices. There is a huge amount of demand for RFBs in the arena of AGC. In this sort of battery, no sensitive material is used in its construction, and it is assisted by an external establishment of stowing containers. Thus, complete energy competence is reliant on the number of electrolytes in exterior stowage containers and production power is associated with the group of electrodes. The electrolytes are a suspension of sulfuric acid in amalgamation with vanadium ions. A duo of pumps is linked to stream the suspension over cells of the battery. The chemical responses which arise internally in battery cells throughout charging in conjunction with discharging are shown in Equations (6) and (7):

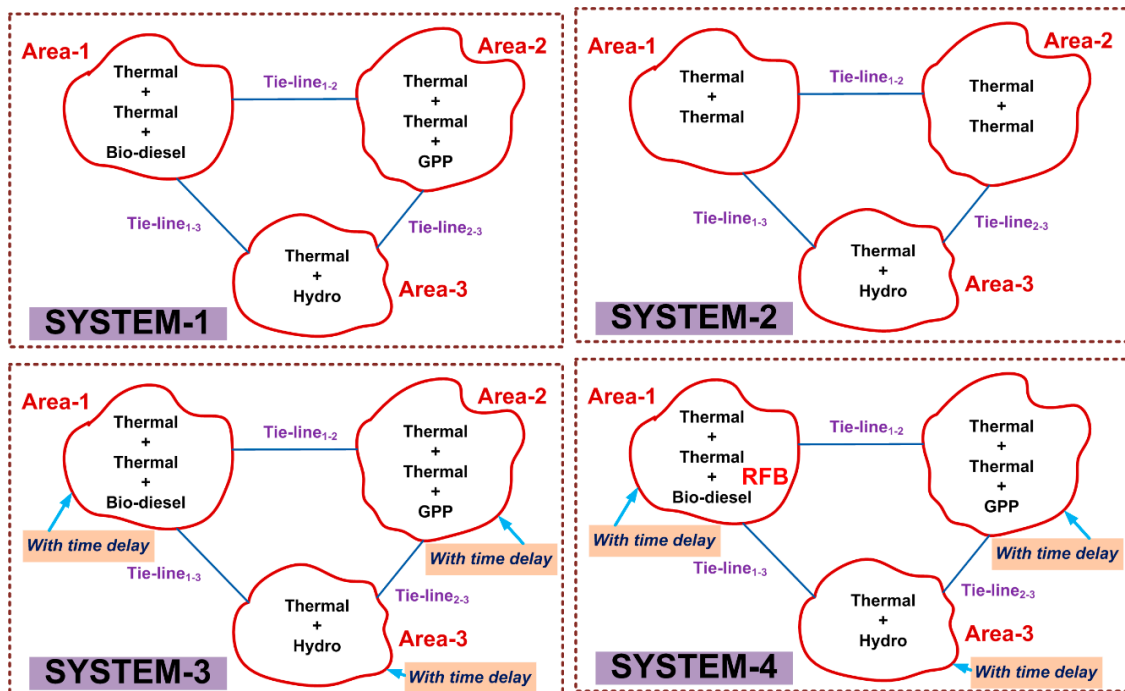
At the site of +ve electrical conductor:



At the site of -ve electrical conductor:

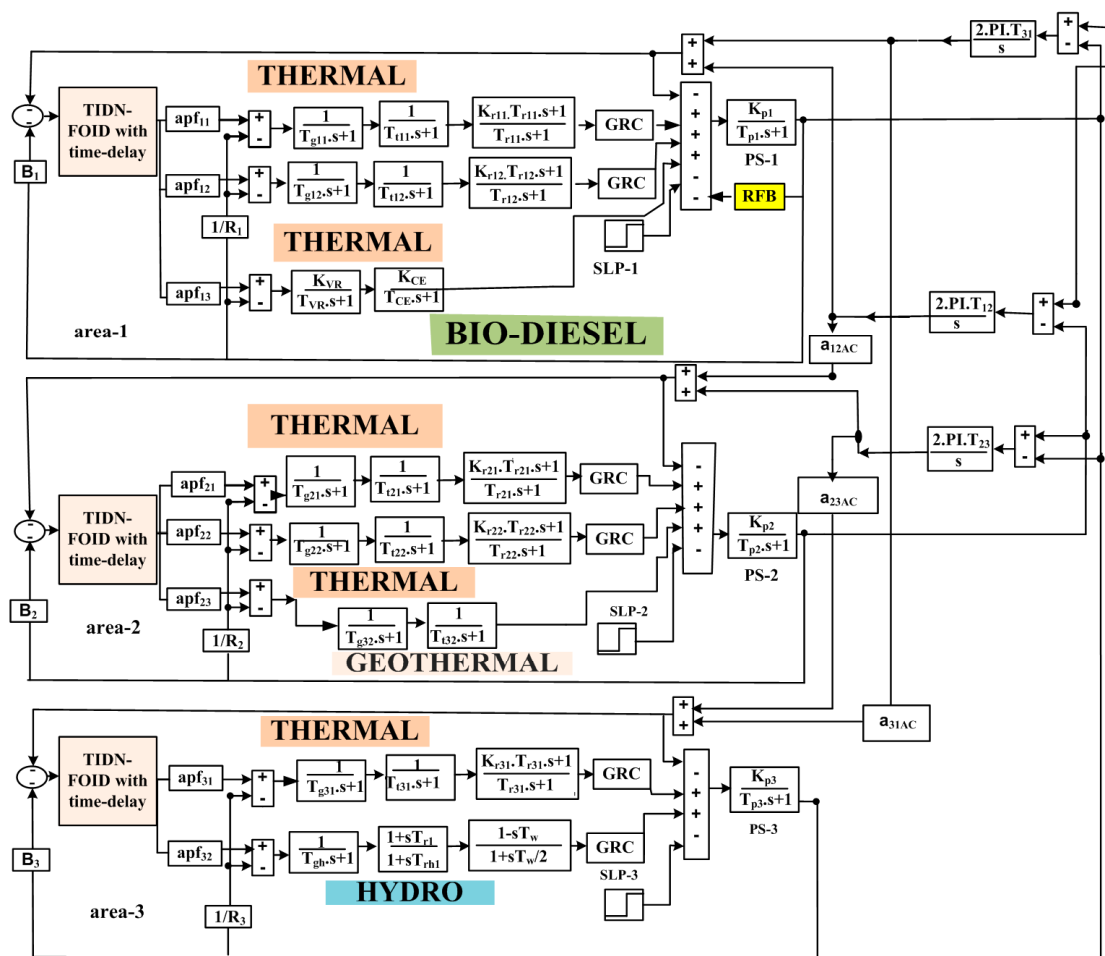


RFB has characteristics of elongated operational duration and huge power capacity. It has certain strengths, such as its quick small-span additional ability, huge efficiency, exposure to autonomous discharge matters, being inexpensive, and not being cluttered by unforeseen changes.

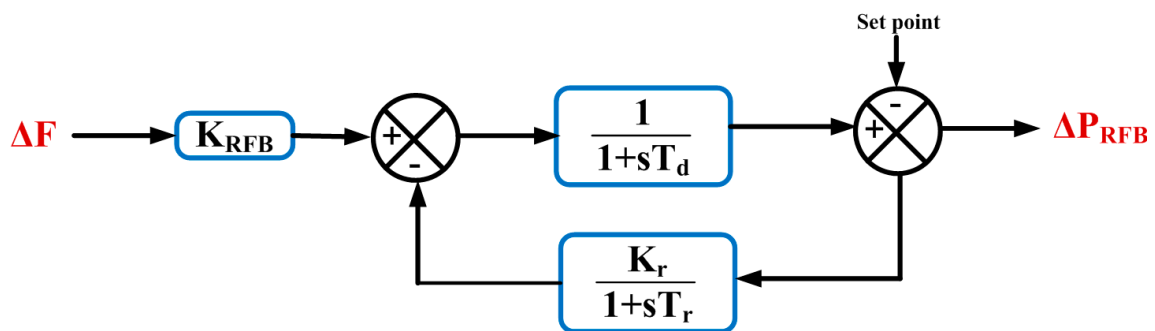


(a)

Figure 1. Cont.



(b)



(c)

**Figure 1.** The schematic and Trfn model of the uneven triple-arena scheme with hydrothermal-biodiesel-GPPt units along with RFB: (a) schematic model of uneven triple-arena scheme with hydrothermal-biodiesel-GPPt units along with RFB, (b) Trfn uneven triple-arena scheme with hydrothermal-biodiesel-GPPt units along with RFB, and (c) Trfn model of RFB.

### 3. Projected Controller

The projected controller is a collective of TIDN and FOID. The arrangement of TIDN-FOID is authenticated in Figure 2. Part-1 (B1) and Part-2 (B2) are the layout of TIDN and FOID, respectively.  $R_{s_i}(s)$  is the predecessor impulse and  $O_{s_i}(s)$  is the consequent impulse for the TIDN-FOID subordinate controller.

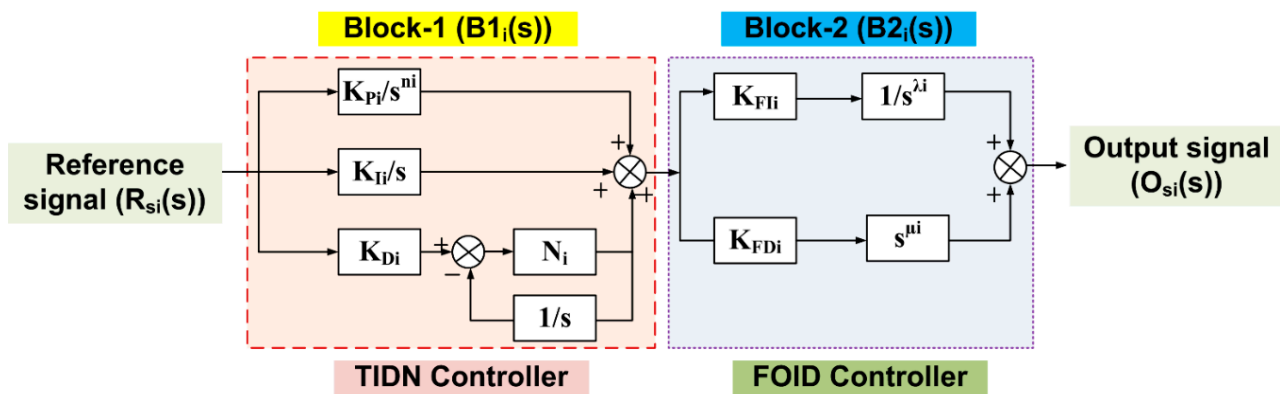


Figure 2. Layout of the proposed controller (TIDN-FOID).

The Riemann–Liouville FRO integral and derivative are shown in Equations (8) and (9) [60]:

$$\alpha D_t^{-\alpha} f(t) = \frac{1}{\Gamma(n)} \int_{\alpha}^t (t - \tau)^{\alpha-1} f(\tau) d\tau, \quad n - 1 \leq \alpha < n, n \text{ is an integer} \quad (8)$$

$$\alpha D_t^{\alpha} f(t) = \frac{1}{\Gamma(n - \alpha)} \frac{d^n}{dt^n} \int_{\alpha}^t (t - \tau)^{n-\alpha-1} f(\tau) d\tau \quad (9)$$

where  $\alpha D_t^{\alpha}$  is the fractional operator and  $\Gamma(\cdot)$  is the Euler’s gamma function. The amendment of above equations in the Laplace domain is given by (10):

$$L\{\alpha D_t^{\alpha} f(t)\} = s^{\alpha} F(s) - \sum_{k=0}^{n-1} s^k \alpha D_t^{\alpha-k-1} f(t)|_{t=0} \quad (10)$$

The detriment of boundless computation of poles and zeros by the feature of absolute semblance is demonstrated by Oustaloup et al. [61]. Here, a convenient Trfn is promulgated, which can be approximated by FrO derivatives collected with integrators through the indentation of recursive dispersal of poles and zeros, as shown in Equation (11):

$$s^{\alpha} = K \prod_{n=1}^M \frac{1 + (s/\omega_{Z,n})}{1 + (s/\omega_{p,n})} \quad (11)$$

where  $K = 1$ , gain = 0 dB over 1 rad/s frequency,  $M$  is the total number of poles besides zeros (obtained previously), and frequency option for poles and zeros are established by Equations (12)–(16):

$$\omega_{Z,l} = \omega_l \sqrt[n]{n} \quad (12)$$

$$\omega_{p,n} = \omega_{Z,n} \varepsilon \quad n = 1, \dots, M \quad (13)$$

$$\omega_{Z,n+1} = \omega_{p,n} \sqrt[n]{\eta} \quad (14)$$

$$\varepsilon = \left( \frac{\omega_h}{\omega_l} \right)^{\frac{v}{M}} \quad (15)$$

$$\eta = \left( \frac{\omega_n}{\omega_l} \right)^{\frac{(1-v)}{M}} \quad (16)$$

The TIDN controller is the modified form of the PIDN controller where the proportional gain is associated with a tilted constituent in the form of  $s^{-(1/n)}$  or  $1/s^{(1/n)}$ . TIDN is chosen as it facilitates hassle free tuning, an excellent ratio of disturbance rejection; it is also the least affected by the alteration of system parameters.

The Trfn of  $B1_i(s)$  is calculated with Equation (17):

$$B1_i(s) = \{K_{Pi}/(s^{1/n_i})\} + \{K_{Ii}/(s)\} + K_{Di} \frac{N_i}{1 + N_i/s} \quad (17)$$

The Trfn of  $B2_i(s)$  is calculated with Equation (18).

$$B2_i(s) = \frac{K_{FIi}}{s^{\lambda_i}} + s^{\mu_i} K_{FDi} \quad (18)$$

where  $\lambda$  and  $\mu$  is the non-integer parameter of the FOID integrator and derivative part individually and  $K_{FIi}$  and  $K_{FDi}$  are the integral and derivative gain of FrO, respectively, of the suggested area.

Henceforth:

$$O_{si}(s) = (B1_i(s)B2_i(s)) * R_{si}(s) \quad (19)$$

The fine-tuning constraints of TIDN and FOID are obtained via SHO by J<sub>ISE</sub> Equation (20):

$$\left\{ \begin{array}{l} K_{Pi}^{\min_{PiPi}^{\max}}, K_{Ii}^{\min_{IiIi}^{\max}}, K_{Di}^{\min_{DiDi}^{\max}}, \\ N_i^{\min_{Ni}^{\max}}, n_i^{\min_{ni}^{\max}}, K_{FIi}^{\min_{FIiFIi}^{\max}}, \\ K_{FDi}^{\min_{FDiFDi}^{\max}}, \lambda_i^{\min_{\lambda_i}^{\max}}, \mu_i^{\min_{\mu_i}^{\max}} \end{array} \right. \quad (20)$$

The specified limitations of frequency  $[\omega_1, \omega_h]$  replicated for valuation is [0.01, 50],  $K_{Pi}$ ,  $K_{Ii}$ ,  $K_{Di}$ ,  $K_{FIi}$ ,  $K_{FDi}$ ,  $\lambda_i$ , and  $\mu_i$  are surrounded by 0–2, values of  $n_i$  are 1–12, and values for  $N_i$  are 0–100. These restrictions are established by exercise and distinct numerary of exploratory.

#### 4. Optimization Approach—Spotted Hyena Optimizer (SHO)

Spotted Hyenas (SHy) are recognized as skilled pursuers, even though they are the largest among the hyaena species. SHy are also well known as the “laughing hyena”, as their vocalizations sound similar to human laughter. They are extremely complicated, intelligent, and social creatures. The SHy trace victims using their highly developed sense of sight, hearing, and smell. This behavior of SHy led Dhiman et al. [57] to develop a meta-heuristic algorithm, i.e., SHO. The authors created an arithmetical strategy based on SHy and mutual dexterity for optimization. The three actions associated with SHO are catch, encircling, and noticeable catch.

- i. Surrounding of catch: To evolve this mathematical archetype, it is expected that the current premium challenger is the intended catch, provided that the pursuit field is recognized formerly. In this pursuit, the catch will be introduced to a location familiar to the pursuit mediator to gain an advantage. An arithmetical sample is demonstrated by Equations (21) and (22):

$$\vec{D}_h = \left| \vec{B} \cdot \vec{P}_p(x) - \vec{P}(x) \right| \quad (21)$$

$$\vec{P}(x+1) = \vec{P}_p(x) - \vec{E} \cdot \vec{D}_h \quad (22)$$

where  $\vec{D}_h$  is the stretch between the prey and SHy,  $x$  is the present count,  $\vec{B}$  and  $\vec{E}$  are vector coefficients,  $\vec{P}_p$  is the spot vector of the hunt,  $\vec{P}$  is the locale vector of Shy, and  $\vec{B}$  and  $\vec{E}$  are calculated by (23)–(25):

$$\vec{B} = 2rd_1 \quad (23)$$

$$\vec{E} = 2hrd_2 - h \quad (24)$$



$$\vec{h} = 5 - (t * (5/t_{\max})) \text{ where } t = 1, 2, 3 \dots, t_{\max} \quad (25)$$

where  $t$  is the number of iterations and  $t_{\max}$  is the maximal number of iterations.

To explore instead of exploit,  $\vec{h}$  in the conventional contour deteriorated on or after 5 towards 0, and concluded towards the end of the maximum number of iterations. Furthermore, this implementation of sanctions increased the amount of exploitation as the total value grew. Nevertheless,  $\vec{r}_{d1}$  besides  $\vec{r}_{d2}$  are random vectors inside  $[0, 1]$ .

- ii. Tricking: With the purpose to portray the demeanor of SHy arithmetically, it is expected that the premium pursuit mediator has data concerning the location of the hunt. The enduring pursuit mediator forms assemblages on the way to the premium pursuit mediator, and stores the premium consequence to reestablish their location, as calculated by Equations (26)–(28):

$$\vec{D}_h = |\vec{B} \cdot \vec{P}_h - \vec{P}(x)| \quad (26)$$

$$\vec{P}_k = \vec{P}_h - \vec{E} \cdot \vec{D}_h \quad (27)$$

$$\vec{C}_h = \vec{P}_k + \vec{P}_{k+1} + \dots + \vec{P}_{k+N} \quad (28)$$

where  $\vec{P}_h$  outlines the locale of preliminary premium SHy and  $\vec{P}_k$  describes the locale of supplementary SHy.  $N$  describes the numeral of SHy as follows:

$$N = \text{count}_{\text{nos}} \left( \vec{P}_h, \vec{P}_{h+1}, \vec{P}_{h+2}, \dots, \left( \vec{P}_h + \vec{M} \right) \right) \quad (29)$$

where  $\vec{M}$  is the arbitrary vector in  $[0.5, 1]$ , nos is the framework of the number of consequences and the entirety of the competitor results, afterwards adding  $\vec{M}$ , which are comparable to the premium perfect consequence in a stated quest arena, and  $\vec{C}_h$  is an assembly of  $N$  numerals of perfect consequence.

- iii. Intruding quest (exploitation): In order to design the prototype on the basis of equations, so as to attack the prey,  $\vec{h}$  numerical measure is diminished. The discrepancy in  $\vec{E}$  is likewise condensed from 5 to 0 with computation.  $|E| < 1$  pressurizes the assemblage of SHy to outbreak on the way to hunt. The mathematical strategy for inflowing the prey is as follows:

$$\vec{P}(x+1) = \frac{\vec{C}_h}{N} \quad (30)$$

where  $\vec{P}(x+1)$  stores the premium product and revises the location of the additional pursuit mediators, consistent with the location of the premium pursuit mediators.

- iv. Hunt for aim (exploration): SHy habitually pursues the prey, according to the location of the SHy, which subsist in  $\vec{C}_h$ . They swing separately to pursue and hunt their prey. Then,  $\vec{E}$  is utilized with random standards  $>1$  or  $<-1$  to coerce the pursuit mediators to swing far away from the prey. This stratagem certifies the SHO algorithm to pursue extensive attainment. SHO's flow diagram is shown in Figure 3.

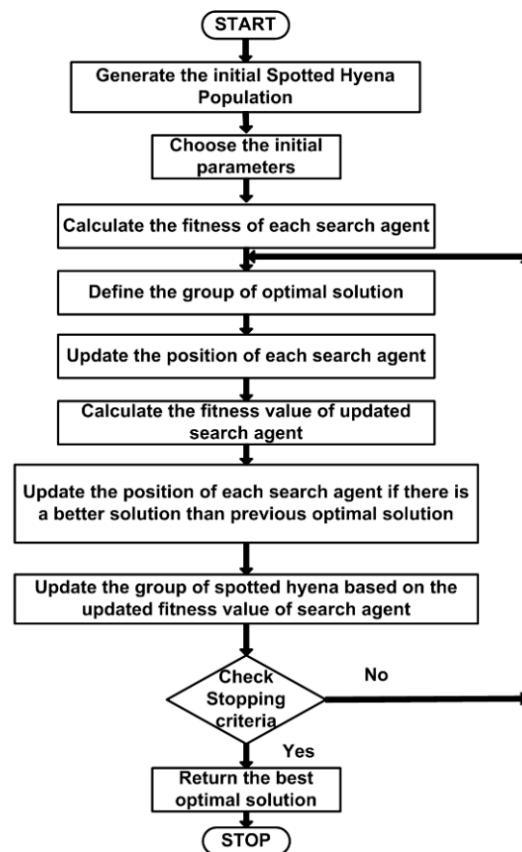


Figure 3. Flowchart of the SHO algorithm.

## 5. Outcomes and Valuation

The optimization algorithms (WOA, CS, FA, and SHO) are programmed in MATLAB2020a and MATLAB2022a (PSO) software, and the system is modeled in Simulink using the FOMCON toolbox. The spotted hyena optimizer algorithm is used to optimize the controller gain parameters.

### 5.1. Valuation of Potent Outcomes for the Choice of Superlative Controller (Including Biodiesel and Geothermal Energy)

The scheme inspected here for valuation embraces T-T-Bd in arena-1, T-T-GPP in arena-2, and T-H in arena-3 (Structure-1). This structure is adapted with PIDN/TIDN/TIDN-FOID subordinate controllers of discrete origin. Valuation is accomplished by including 1% step load tolerances in arena-1. The superlative accessible values of the respective controller's attributes are attained via SHO, with  $P_{iSE}$ . The structure is first and foremost adapted with the PIDN subordinate controller to acquire its attributes as well as the attributes of GPPt via SHO. The governor and turbine time constants gained is 0.1 s. The standards of  $G_{GPPt}$  and  $T_{GPPt}$  are similar in the rest of the paper. After that, TIDN and TIDN-FOID subordinate controllers are applied autonomously. The premium probable values are manifested in Table 1, and with these, potential outcomes are acquired, as shown in Figure 4. Extensive analysis of respective outcomes articulates the distinction of TIDN-FOID over added controllers concerning the narrowed level of crowning\_overshoot (C\_O), degree-of-fluctuations, and crowning\_undershoot (C\_U) in addition to the extent of settling duration (S\_D). In Table 2, the equivalent figures C\_O, C\_U, and S\_D values are displayed, showing the enhanced presentation of TIDN-FOID over PIDN and TIDN.

**Table 1.** Premium values of attributes of PIDN, TIDN, and TIDN-FOID subordinate controllers for the scheme including biodiesel and GPpT.

Name of Controller	Corresponding Gains and Parameters	Area-1	Area-2	Area-3
PIDN	$K_{Pi}^*$	0.0016	0.0025	0.0027
	$K_{Ii}^*$	0.3784	0.4651	0.5068
	$K_{Di}^*$	0.4882	0.3788	0.3569
	$N_i^*$	12.11	13.01	15.00
TIDN	$K_{Pi}^*$	0.1532	0.4706	0.3715
	$K_{Ii}^*$	0.4888	0.4426	0.5827
	$K_{Di}^*$	0.8056	0.6795	0.5687
	$N_i^*$	45.01	56.11	38.21
	$n_i^*$	1.4091	2.5088	2.1078
TIDN-FOID	$K_{Pi}^*$	0.5470	0.7826	0.8511
	$K_{Ii}^*$	0.6584	0.7650	0.8756
	$K_{Di}^*$	0.8033	0.8862	0.9617
	$N_i^*$	92.08	85.82	82.68
	$n_i^*$	3.9977	2.8985	1.1748
	$K_{FIi}^*$	0.4707	0.3868	0.4477
	$\lambda_i^*$	0.0020	0.0082	0.0021
	$K_{FDi}^*$	0.7356	0.4747	0.5937
	$\mu_i^*$	0.0722	0.0259	0.0473

\* Signify the optimum values.

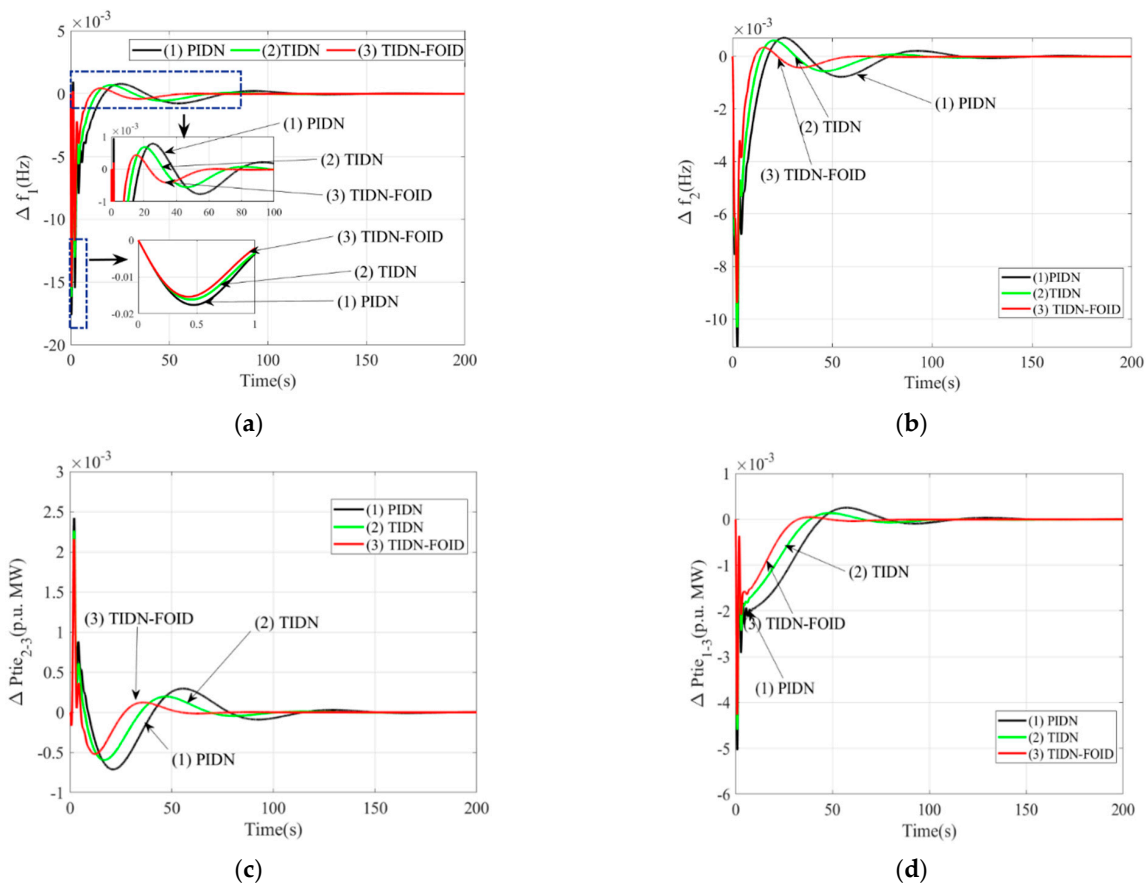


**Figure 4.** Valuation of consequences of subsidiary controllers PIDN, TIDN, and TIDN-FOID for structure-1 (including biodiesel and GPpT) for 1% step load tolerances disparity time: (a) arena-1 frequency anomaly, (b) arena-2 frequency anomaly, (c) anomaly in power interrelating arena-2 and -3, and (d) anomaly in power interrelating arena-1 and -3.

**Table 2.** C\_O, C\_U, and S\_D for consequences in Figure 4 in circumstance of structure-1 using SHO-augmented PIDN/TIDN/TIDN-FOID subordinate controllers.

Responses	Name of Controller	C_O	C_U	S_D (In Seconds)
$\Delta f_1$ (Figure 4a)	PIDN	0.0008	0.0176	118.10
	TIDN	0.0006	0.0161	98.72
	TIDN-FOID	<b>0.0004</b>	<b>0.0153</b>	<b>62.36</b>
$\Delta f_2$ (Figure 4b)	PIDN	0.0007	0.0110	111.50
	TIDN	0.0005	0.0103	89.71
	TIDN-FOID	<b>0.0003</b>	<b>0.0093</b>	<b>57.44</b>
$\Delta P_{tie_{2-3}}$ (Figure 4c)	PIDN	0.0024	0.0007	119.30
	TIDN	0.0022	0.0006	100.81
	TIDN-FOID	<b>0.0021</b>	<b>0.0004</b>	<b>57.37</b>
$\Delta P_{tie_{1-3}}$ (Figure 4d)	PIDN	0.0002	0.0051	109.11
	TIDN	0.0001	0.0045	88.27
	TIDN-FOID	<b>0.00004</b>	<b>0.0042</b>	<b>56.69</b>

*Bold signifies best values.*

### 5.2. Suggestion of $P_{ix}$

The leading performance index ( $P_{ix}$ ) among the integral squared error ( $P_{ix_{ISE}}$ ), integral absolute error ( $P_{ix_{IAE}}$ ), integral time squared error ( $P_{ix_{ITSE}}$ ), and integral time absolute error ( $P_{ix_{ITAE}}$ ) is acquired by facilitating structure-1, excluding these  $P_{ix}$  on individual terms via the TIDN-FOID controller. The finest values of the TIDN-FOID controller's attributes are accomplished via the SHO algorithmic procedure. The expression of  $P_{ix_{ITSE}}$ ,  $P_{ix_{IAE}}$ , and  $P_{ix_{ITAE}}$  are shown in Equations (31)–(33), respectively, while the expression of  $P_{ix_{ISE}}$  was shown by Equation (5):

$$P_{ix_{ITSE}} = \int_0^T \left\{ (\Delta f_1)^2 + (\Delta f_2)^2 + (\Delta f_3)^2 + (\Delta P_{tie_{1-2}})^2 + (\Delta P_{tie_{2-3}})^2 + (\Delta P_{tie_{1-3}})^2 \right\} t \, dt \quad (31)$$

$$P_{ix_{IAE}} = \int_0^T \left\{ |\Delta f_1| + |\Delta f_2| + |\Delta f_3| + |\Delta P_{tie_{1-2}}| + |\Delta P_{tie_{2-3}}| + |\Delta P_{tie_{1-3}}| \right\} dt \quad (32)$$

$$P_{ix_{ITAE}} = \int_0^T \left\{ |\Delta f_1| + |\Delta f_2| + |\Delta f_3| + |\Delta P_{tie_{1-2}}| + |\Delta P_{tie_{2-3}}| + |\Delta P_{tie_{1-3}}| \right\} t \, dt \quad (33)$$

Using the best values obtained for TIDN-FOID controller in individual circumstances, the potent outcomes are distinguished in Figure 5a–c. In addition, the conforming C\_O and C\_U, besides S\_D standards, are shown in Table 3. An extensive understanding of the outcomes shows that outcomes using  $P_{ix_{ISE}}$ , as per  $P_{ix}$ , have a healthier presentation with reference to diminished C\_O, C\_U, and S\_D oscillations. Additionally, the standards of  $P_{ix}$  are  $P_{ix_{ISE}} = 0.0007218$ ,  $P_{ix_{ITSE}} = 0.001793$ ,  $P_{ix_{IAE}} = 0.1467$ , and  $P_{ix_{ITAE}} = 1.3210$ , showing that  $P_{ix_{ISE}}$  improves the scheme. The merging features for structure-1 via dissimilar  $P_{ix}$  are shown in Figure 5d. It can be seen that merging features via ISE as  $P_{ix}$  converges quicker in fewer repetitions when more  $P_{ix}$ s are added.

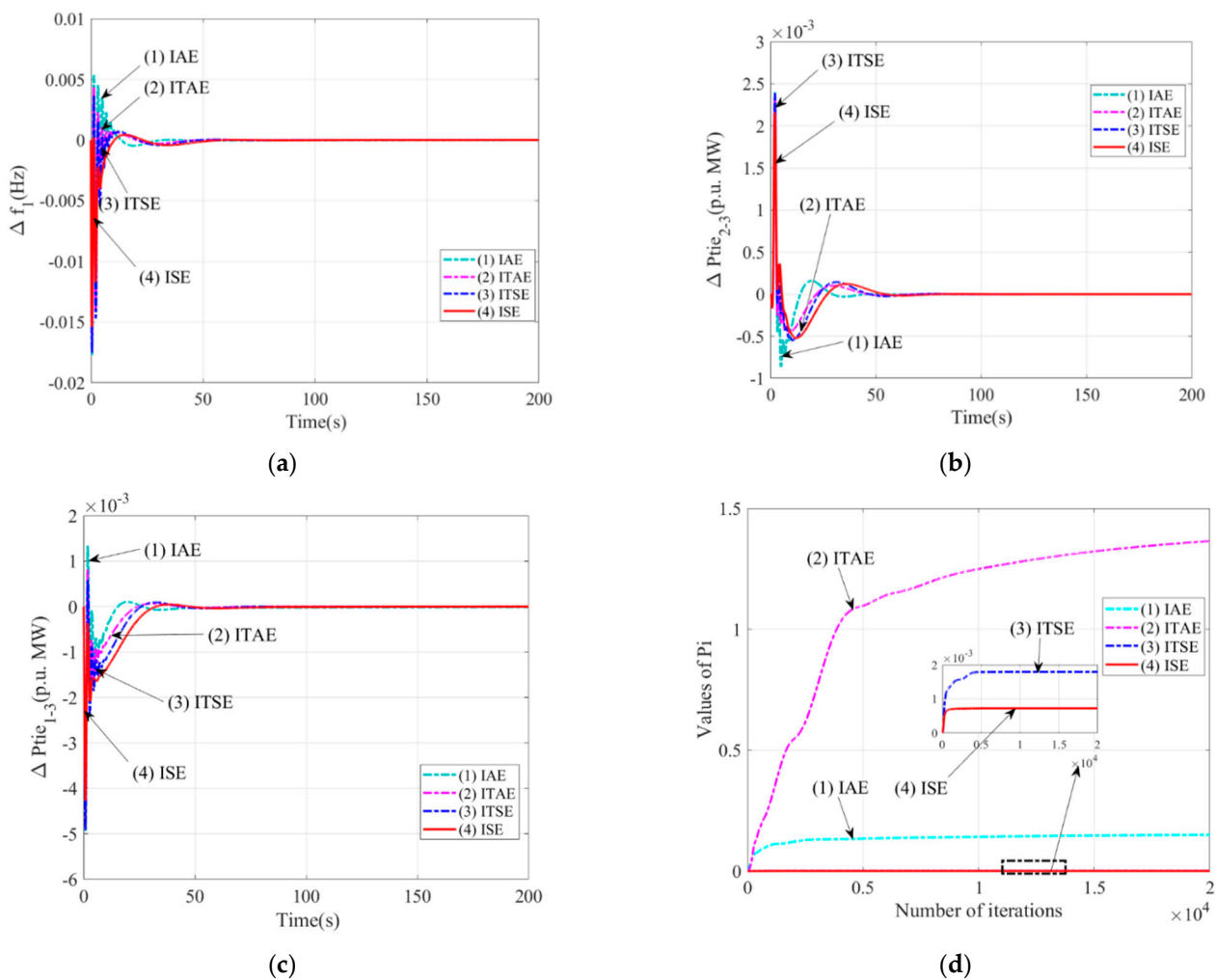


**Figure 5.** Assessment for the nomination of performance index ( $PI_x$ ) for IAE, ITSE, ITAE, and ISE using the TIDN-FOID subordinate controller using structure-1: (a) arena-1 frequency anomaly, (b) anomaly in power interrelating arena-2 and -3, (c) anomaly in power interrelating arena-1 and -3, and (d) converging curvature for structure with dissimilar  $Pi$ .

**Table 3.**  $C_O$ ,  $C_U$ , and  $S_D$  for the results in Figure 5a–c for structure-1 via an SHO-augmented TIDN-FOID subordinate controller for different performance indices.

Outcomes	Performance Indices	$C_O$	$C_U$	$S_D$ (In Seconds)
$\Delta f_1$ (Figure 5a)	IAE	0.0053	0.0176	72.97
	ITAE	0.0041	0.0171	69.82
	ITSE	0.0036	0.0175	68.85
	<b>ISE</b>	<b>0.0004</b>	<b>0.0153</b>	<b>62.36</b>
$\Delta Ptie_{2-3}$ (Figure 5b)	IAE	0.0023	0.0008	70.39
	ITAE	0.0023	0.0005	70.05
	ITSE	0.0024	0.0005	66.04
	<b>ISE</b>	<b>0.0021</b>	<b>0.0004</b>	<b>57.37</b>
$\Delta Ptie_{1-3}$ (Figure 5c)	IAE	0.0013	0.0048	66.89
	ITAE	0.0008	0.0047	66.87
	ITSE	0.0005	0.0046	64.67
	<b>ISE</b>	<b>0.00004</b>	<b>0.0042</b>	<b>56.69</b>

*Bold signifies best values.*

### 5.3. Suggestion of Optimization Procedure

For the algorithm, the structure-1 is furnished with dissimilar algorithms distinctly via TIDN-FOID subordinate controllers. The optimization procedure adopted here are WOA, PSO [50,51], CS [52], FA, and SHO. For WOA, the number of search individuals equals 51 and the number of iterations equals 100. In case of PSO, the adjusted constraints standards remain at  $\omega = 1.1$ ,  $\omega_{damppe} = 0.98$ ,  $c_1 = 1.38$ ,  $c_2 = 1.97$ , population size equal 54, and the extreme maximum number of iterations equals 100. In case of CS, nests amount = 51, rate of detection = 0.51, exponent of levy = 1.49, supreme generation = 100, and sum of extents = 11. The tuned values for FA are  $\beta_0 = 0.29$ ,  $\alpha = 0.51$ ,  $\gamma = 0.42$ , sum of fireflies = 51, and supreme figure of iterations = 100. For every algorithm, the superlative values for the TIDN-FOID subordinate controller are attained. The standards are not provided here. Through these standards, the outcomes of the diverse algorithms are distinguished in Figure 6a–c. The conforming outcomes C\_O, C\_U, and S\_D standards are specified in Table 4, where it can be realized that C\_O, C\_U, S\_D, and computational values obtained by the SHO-augmented TIDN-FOID subordinate controller are significantly improved compared to the added algorithmic procedure. Additionally, the dominance is arbitrated by the conjunction curvature shown in Figure 6d, where it is detected that outcomes with the SHO-augmented TIDN-FOID subordinate controller converges quicker and have a minimum value of  $PIx_{ISE}$ . Consequently, supplementary analysis is supported via the SHO algorithmic procedure.

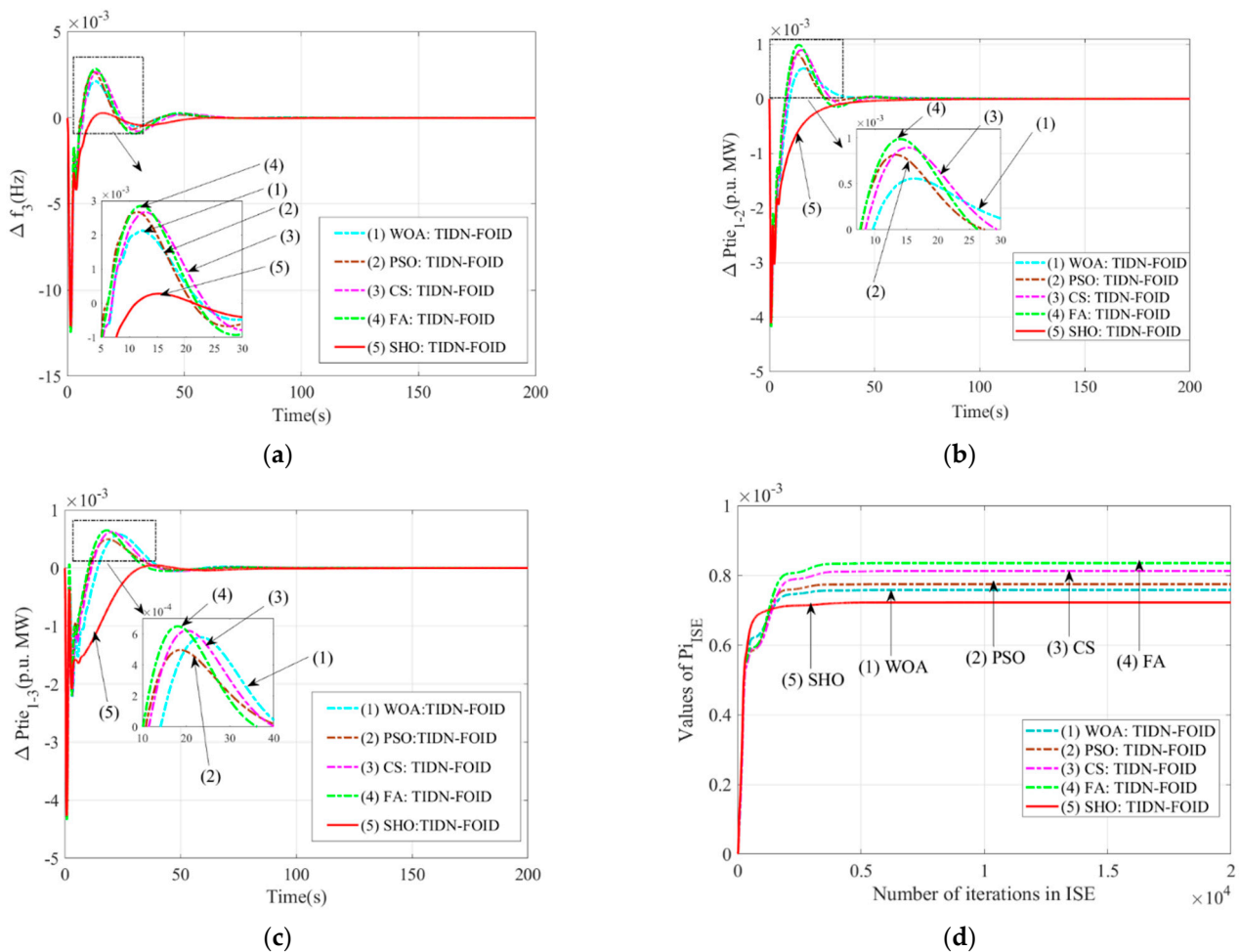


**Figure 6.** Valuation for the reference of the algorithm within WOA/PSO/CS/FA/SHO procedures for the procurement of premium values of the TIDN-FOID subordinate controller for structure-1: (a) arena-2 frequency anomaly, (b) anomaly in power interrelating arena-1 and -2, (c) anomaly in power interrelating arena-1 and-3, and (d) convergence curve.

**Table 4.** P\_O, P\_U, and S\_T for dynamics in Figure 6 in case of structure-1 using a WOA/PSO/CS/FA/SHO-augmented TIDN-FOID subordinate controller on an individual base.

Responses	Name of Algorithm	C_O	C_U	S_D (In Seconds)	Computational Time (In Seconds)
$\Delta f_3$ (Figure 6a)	WOA	0.0021	0.0120	60.28	380
	PSO	0.0026	0.0122	65.31	375
	CS	0.0026	0.0121	66.39	378
	FA	0.0028	0.0124	67.64	353
	<b>SHO</b>	<b>0.0002</b>	<b>0.0120</b>	<b>54.92</b>	<b>310</b>
$\Delta P_{tie1-2}$ (Figure 6b)	WOA	0.0005	0.0042	62.32	380
	PSO	0.0008	0.0042	71.01	375
	CS	0.0009	0.0042	68.09	378
	FA	0.0009	0.0042	66.87	353
	<b>SHO</b>	<b>0</b>	<b>0.0041</b>	<b>50.72</b>	<b>310</b>
$\Delta p_{tie1-3}$ (Figure 6c)	WOA	0.0005	0.0043	80.28	380
	PSO	0.0005	0.0043	78.28	375
	CS	0.0006	0.0043	80.68	378
	FA	0.0006	0.0044	67.87	353
	<b>SHO</b>	<b>0.00004</b>	<b>0.0042</b>	<b>56.69</b>	<b>310</b>

*Bold signifies best values.*

#### 5.4. Valuation of the Influence of Biodiesel and GPpT on the Dynamics of the System

In Section 5.1, it was shown that the performance of the SHO-augmented TIDN-FOID controller is better compared to PIDN/TIDN controllers. The system in Section 5.1 included both biodiesel as well as GPP. Now, in order to analyze the impact of biodiesel and GPpT on system dynamics, they are removed from structure-1, keeping the capacities of the areas constant. Thus, the system now has thermal-thermal energy in area-1 and area-2 and hydrothermal energy in area-3 (structure-2). For structure-2, the best values of the TIDN-FOID controller are shown in Table 5, obtained by using the SHO controller. With these values, the responses for with and without both biodiesel and GPpT are contrasted in Figure 7. It can be easily viewed that the system in presence of biodiesel and GPpT have a large number of lessened values of peak\_overshoot, peak\_undershoot, settling\_time, and number of oscillations. Only four responses are provided here.

**Table 5.** Best values of attributes of TIDN-FOID controllers for structure-2 (hydrothermal system), excluding biodiesel and GPpT.

Name of Controller	Corresponding Gains and Parameters	Area-1	Area-2	Area-3
TIDN-FOID	$K_{pi}^*$	0.0762	0.0274	0.0385
	$K_{li}^*$	0.3913	0.3850	0.3913
	$K_{Di}^*$	0.7666	0.4598	0.1361
	$N_i^*$	66.72	84.07	95.12
	$n_i^*$	1.8853	3.8440	2.5914
	$K_{Fli}^*$	0.4189	0.8526	0.9492
	$\lambda_i^*$	0.0084	0.0058	0.0037
	$K_{FDi}^*$	0.9043	0.8201	0.7264
	$\mu_i^*$	0.0050	0.0065	0.0032

\* Signify the optimum values.

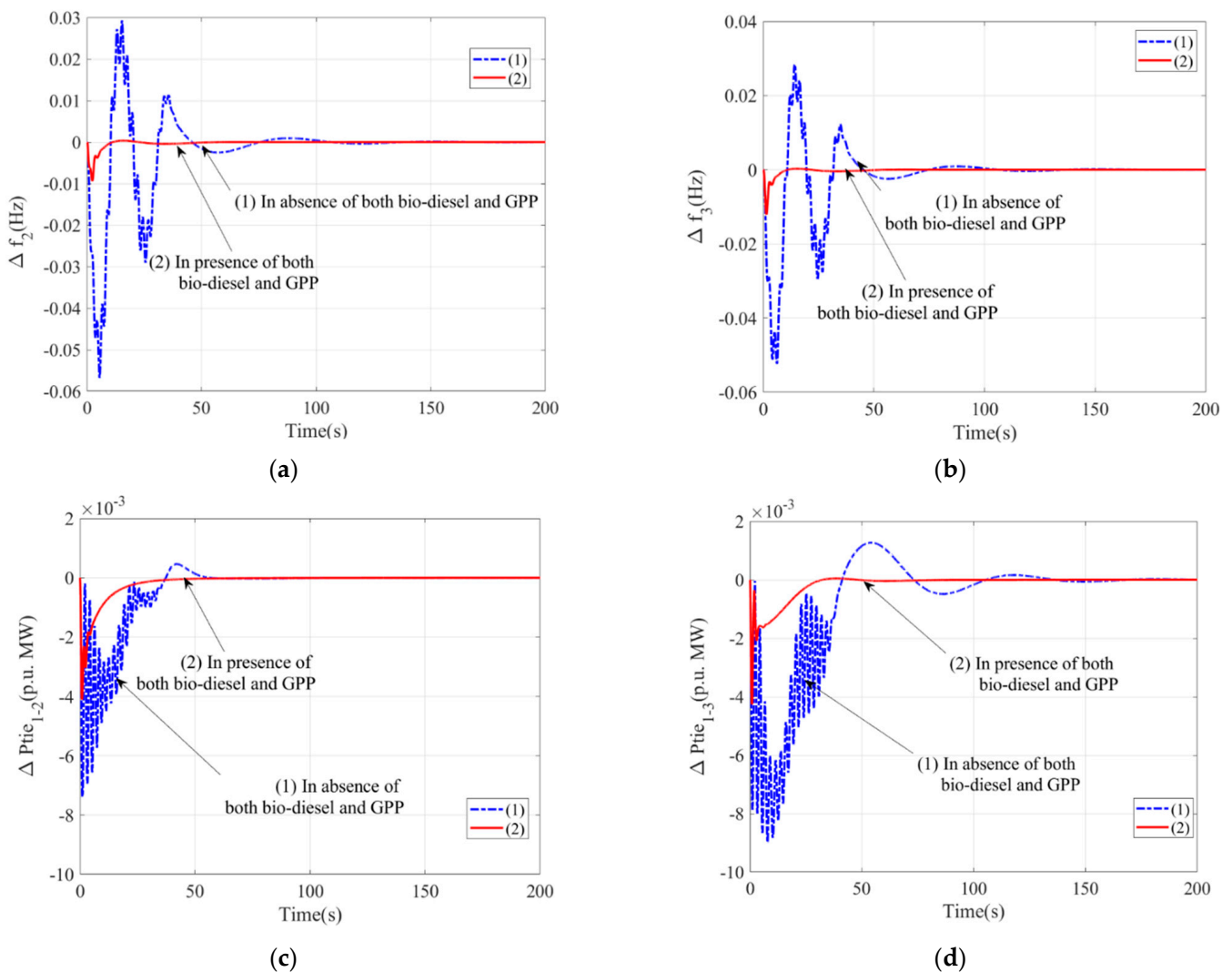


**Figure 7.** Estimation of combined effect of biodiesel and GPpT on scheme potency via SHO-augmented TIDN-FOID subordinate controller using 1% step load tolerances: (a) arena-2 frequency anomalies, (b) arena-3 frequency anomalies, (c) anomaly in power interrelating arena-1 and -2, and (d) anomaly in power interrelating arena-1 and -3.

### 5.5. Valuation of the Influence of Time Delay on the Potency of the Scheme including Biodiesel and GPpT

In the above subsection, it is observed that the presence of biodiesel and GPpT in the system has a noteworthy influence on the system dynamics. Now, the system with biodiesel and GPpT is included with non-linearity time delay ( $\tau_d$ ) in all the areas. Here,  $\tau_d$  is considered varied in different areas, i.e.,  $\tau_{d1} = 0.3$  s in area-1,  $\tau_{d2} = 0.2$  s in area-2, and  $\tau_{d3} = 0.1$  s in area-3. The superlative values of attributes of TIDN-FOID controller via SHO is provided in Table 6. Through these standards, the outcomes are distinguished in Figure 8 for the system with and without time delay. As per our current understanding of each outcome, the incorporation of time delay degrades the system. However, in order to make the system reflect real-world conditions, the association of time delay is needed; hence, the rest of the assessments are performed in the presence of time delay. Only four responses are provided here.



**Table 6.** Best values of attributes of TIDN-FOID subordinate controllers for structure-3 (i.e., including biodiesel, GPPT, and time delay ( $\tau_d$ )).

Name of Controller	Corresponding Gains and Parameters	Area-1	Area-2	Area-3
TIDN-FOID	$K_{p_i}^*$	0.7849	0.8416	0.9610
	$K_{i_i}^*$	0.2748	0.6100	0.2748
	$K_{D_i}^*$	0.8866	0.6639	0.6137
	$N_i^*$	64.66	45.11	70.88
	$n_i^*$	4.5528	5.4326	6.5170
	$K_{FDi}^*$	0.8555	0.4074	0.8386
	$\lambda_i^*$	0.9755	0.7028	0.2556
	$K_{FDi}^*$	0.5163	0.3872	0.5575
	$\mu_i^*$	0.9689	0.6345	0.6229

\* Signify the optimum values.

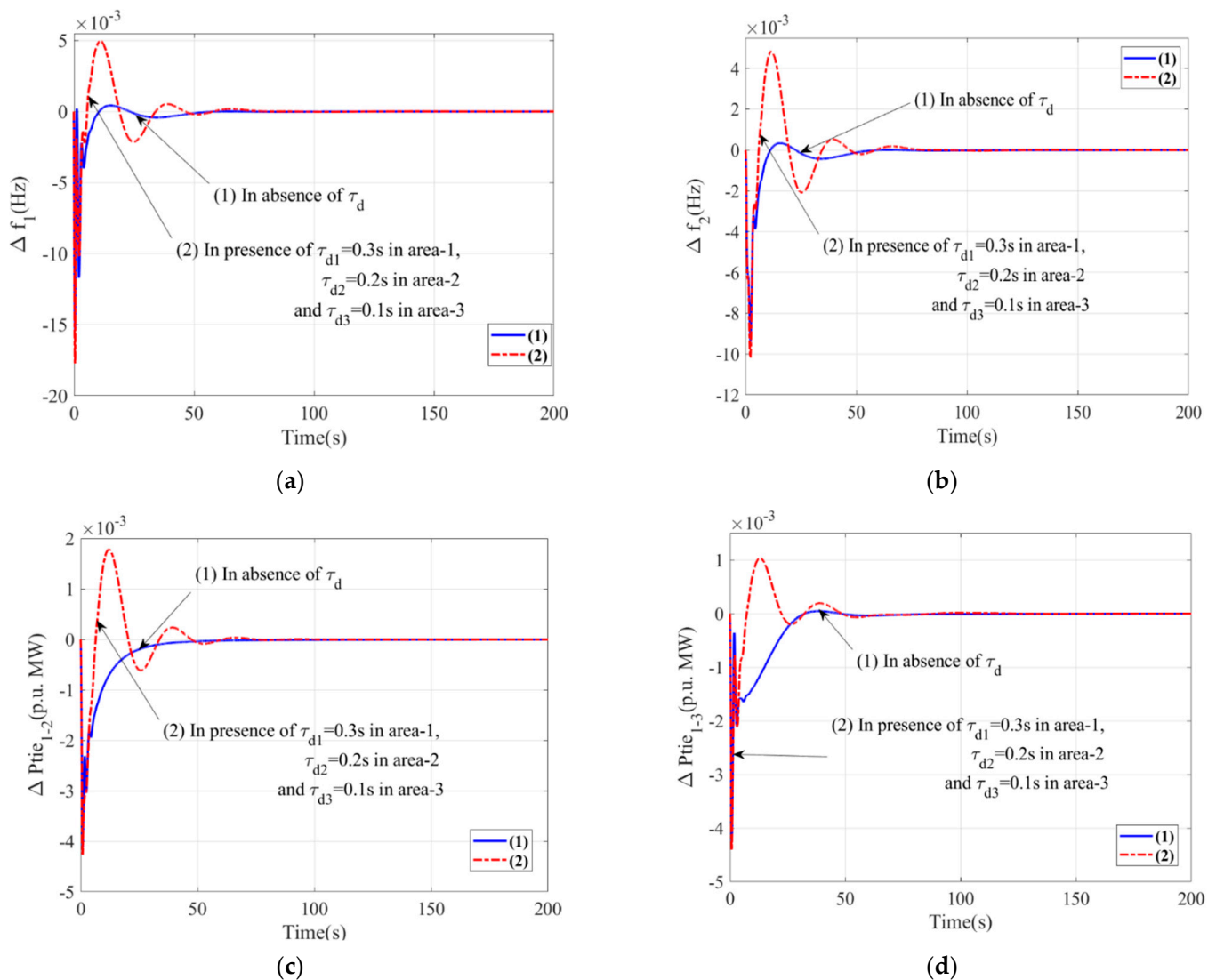


**Figure 8.** Estimation of the impact of time delay on scheme potency via SHO-augmented TIDN-FOID subordinate controller using 1% step load turbulences for scheme-3 ( $\tau_{d1} = 0.3$  s in area-1,  $\tau_{d2} = 0.2$  s in area-2, and  $\tau_{d3} = 0.1$  s in area-3): (a) arena-1 frequency anomalies, (b) arena-2 frequency anomalies, (c) anomaly in power interrelating arena-1 and 2, (d) anomaly in power interrelating arena-1 and 3.

### 5.6. Valuation of the Influence of RFB on the Potency of the Scheme, including Biodiesel and GPP, with Time Delay

In this subsection, the influence of redox flow battery (RFB) is inspected by associating its outcomes with the outcomes of scheme-3 (i.e., a system with T-T-Bd in arena-1, T-T-GPPt in arena-2, and T-H in arena-3, with time delay). TIDN-FOID is considered a subordinate controller. The premium values of attributes of the TIDN-FOID subordinate controller for the scheme in the existence of RFB are shown in Table 7. For these values, the outcomes for the scheme with and without RFB are distinguished in Figure 9. Intensive clarification of each outcome demonstrates the excellence of the scheme potency with the existence of RFB, concerning the diminished level of C\_O, C\_U, and S\_D via the TIDN-FOID controller with 1% step load disturbance in the presence of time delay. Only four responses are provided here.

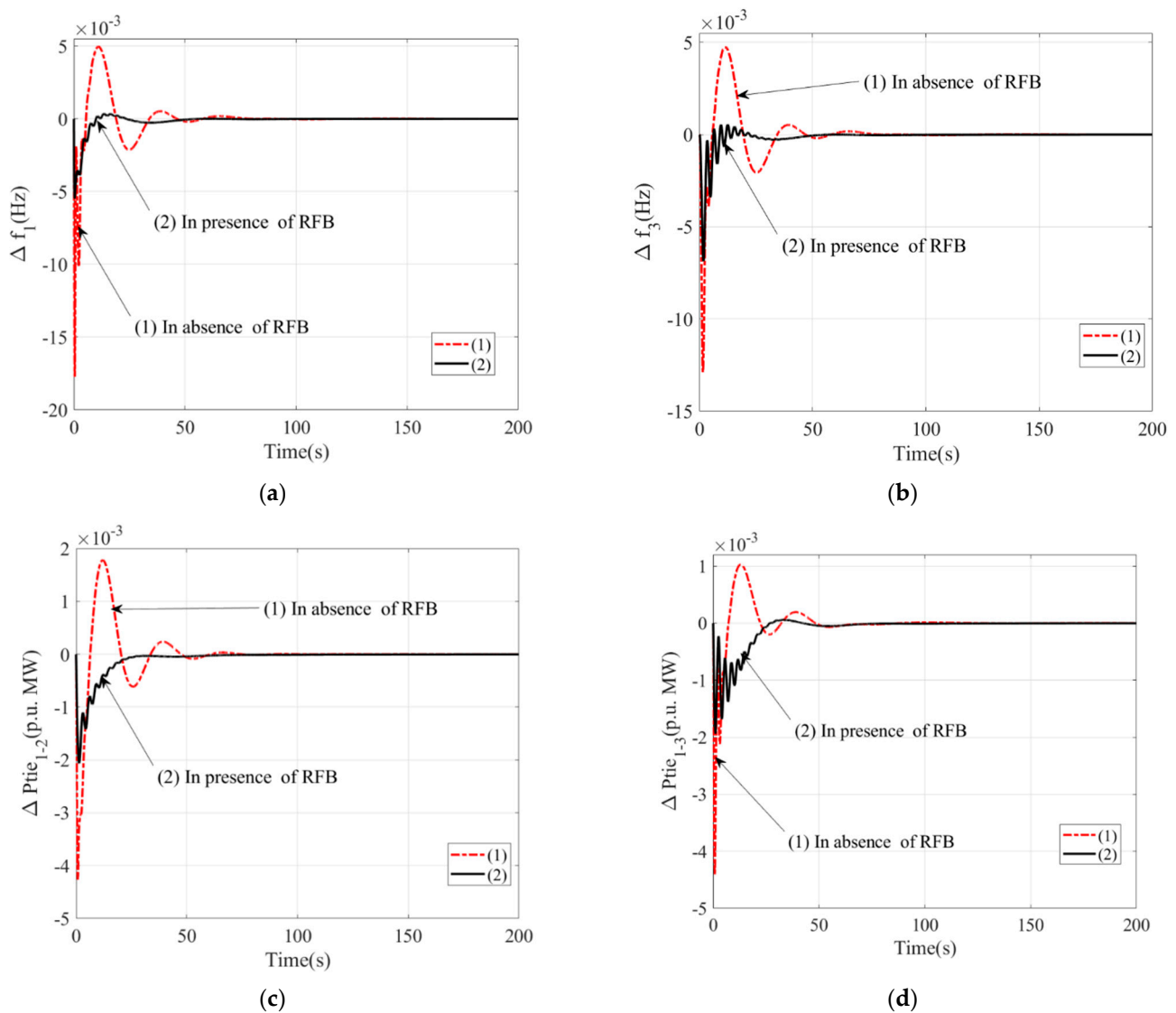


**Figure 9.** Estimation of impact of RFB on scheme potency involving the SHO-augmented TIDN-FOID subordinate controller using 1% step load turbulences for structure-4: (a) arena-1 frequency anomaly, (b) arena-2 frequency anomalies, (c) anomaly in power interrelating arena-1 and -2, and (d) anomaly in power interrelating arena-1 and -3.

**Table 7.** Superlative values of attributes of TIDN-FOID subordinate controllers for structure-4 (i.e., including biodiesel, GPpt, time delay ( $\tau_d$ ), and RFB).

Name of Controller	Corresponding Gains and Parameters	Area-1	Area-2	Area-3
TIDN-FOID	$K_{Pi}^*$	0.6852	0.7387	0.7125
	$K_{Ii}^*$	0.7961	0.8147	0.8922
	$K_{Di}^*$	0.3798	0.4698	0.5863
	$N_i^*$	60.25	65.23	59.11
	$n_i^*$	1.9852	2.3481	3.1520
	$K_{Fli}^*$	0.8513	0.8615	0.8789
	$\lambda_i^*$	0.0328	0.0385	0.0415
	$K_{FDi}^*$	0.8147	0.8789	0.8459
	$\mu_i^*$	0.1614	0.2078	0.2956

\* Signify the optimum values.

### 5.7. Eigenvalue Assessment

In the present subsection, eigenvalue assessment is executed for stability assessment of the system using TIDN-FOID as a secondary controller. Here, the analysis is performed on an individual basis considering two systems: structure-2 (excluding biodiesel, GPpt, time delay, and RFB) and structure-4 (including biodiesel, GPpt, time delay, and RFB). The eigenvalues are shown in Table 8 (for structure-1) and Table 9 (for structure-4). For the eigenvalues in Table 8, it can be seen that the few values marked in blue contain positive real parts, which shows that the structure-2 is unstable. However, in Table 9, there are no positive real parts, so structure-4 is stable compared to structure-2. In Table 10, it can be seen that the minimum damping ratio ( $\xi$ ) is  $\xi = 0.0085$  for structure-1 and  $\xi = 0.0903$  for structure-4. Thus, structure-4 with the TIDN-FOID controller reaches a stable situation faster.

**Table 8.** Eigenvalues of the system in absence of biodiesel, GPpt, time delay, and RFB (structure-2).

System Condition	Eigenvalues
Hydrothermal system excluding biodiesel and GPpt, time delay, and RFB	$-0.1000 + 0.0000i$ $-3.3333 + 0.0000i$ $-0.1000 + 0.0000i$ $-3.3333 + 0.0000i$ $-0.1000 + 0.0000i$
	$-3.3333 + 0.0000i$ $-0.1000 + 0.0000i$ $-3.3333 + 0.0000i$ $-0.1000 + 0.0000i$ $-3.3333 + 0.0000i$
	$-12.5000 + 0.0000i$ $-12.5000 + 0.0000i$ $-12.5000 + 0.0000i$ $-12.5000 + 0.0000i$ $-50.0000 + 0.0000i$
	$-0.0148 + 0.0000i$ $-0.0320 + 0.0000i$ $-0.0695 + 0.0000i$ $-0.1507 + 0.0000i$ $-0.3268 + 0.0000i$
	$-0.7089 + 0.0000i$ $-1.5377 + 0.0000i$ $-3.3353 + 0.0000i$ $-7.2344 + 0.0000i$ $-15.6918 + 0.0000i$
	$-34.0363 + 0.0000i$ $-50.0000 + 0.0000i$ $-0.0147 + 0.0000i$ $-0.0319 + 0.0000i$ $-0.0691 + 0.0000i$
	$-0.1500 + 0.0000i$ $-0.3253 + 0.0000i$ $-0.7055 + 0.0000i$ $-1.5303 + 0.0000i$ $-3.3192 + 0.0000i$
	$-7.1995 + 0.0000i$ $-15.6161 + 0.0000i$ $-33.8722 + 0.0000i$ $-50.0000 + 0.0000i$ $-0.0133 + 0.0000i$
	$-0.0289 + 0.0000i$ $-0.0627 + 0.0000i$ $-0.1359 + 0.0000i$ $-0.2948 + 0.0000i$ $-0.6394 + 0.0000i$
	$-1.3868 + 0.0000i$ $-3.0080 + 0.0000i$ $-6.5246 + 0.0000i$ $-14.1522 + 0.0000i$ $-30.6969 + 0.0000i$
	$0.0000 + 0.0000i$ $-84.0734 + 0.0000i$ $-12.5000 + 0.0000i$ $-50.0000 + 0.0000i$ $-0.0148 + 0.0000i$
	$-0.0320 + 0.0000i$ $-0.0694 + 0.0000i$ $-0.1506 + 0.0000i$ $-0.3266 + 0.0000i$ $-0.7085 + 0.0000i$
	$-1.5367 + 0.0000i$ $-3.3333 + 0.0000i$ $-7.2301 + 0.0000i$ $-15.6824 + 0.0000i$ $-34.0160 + 0.0000i$
	$-50.0000 + 0.0000i$ $-0.0147 + 0.0000i$ $-0.0318 + 0.0000i$ $-0.0691 + 0.0000i$ $-0.1498 + 0.0000i$
	$-0.3249 + 0.0000i$ $-0.7048 + 0.0000i$ $-1.5288 + 0.0000i$ $-3.3160 + 0.0000i$ $-7.1925 + 0.0000i$
	$-15.6009 + 0.0000i$ $-33.8392 + 0.0000i$ $0.0000 + 0.0000i$ $-50.0000 + 0.0000i$ $-66.7220 + 0.0000i$
	$-0.0120 + 0.0000i$ $-0.0260 + 0.0000i$ $-0.0564 + 0.0000i$ $-0.1224 + 0.0000i$ $-0.2655 + 0.0000i$
	$-0.5758 + 0.0000i$ $-1.2490 + 0.0000i$ $-2.7092 + 0.0000i$ $-5.8764 + 0.0000i$ $-12.7463 + 0.0000i$
	$-27.6473 + 0.0000i$ $-95.0002 + 0.0000i$ $-50.2462 + 0.0000i$ $-49.9885 + 0.0000i$ $-33.9013 + 0.0000i$
	$-33.9915 + 0.0000i$ $-50.0000 + 0.0000i$ $-29.2381 + 0.0000i$ $-13.4794 + 0.0000i$ $-15.6295 + 0.0000i$
	$-15.6712 + 0.0000i$ $-6.2134 + 0.0000i$ $-7.2248 + 0.0000i$ $-7.2059 + 0.0000i$ $0.0603 + 2.7150i$
	$0.0603 - 2.7150i$ $-2.8395 + 0.0634i$ $-2.8395 - 0.0634i$ $-3.3236 + 0.0000i$ $-3.3298 + 0.0000i$
	$-1.3369 + 0.0000i$ $-1.1466 + 0.0000i$ $-1.5306 + 0.0000i$ $-1.5362 + 0.0000i$ $-0.0250 + 2.9529i$
	$-0.0250 - 2.9529i$ $-0.7076 + 0.0000i$ $-0.6062 + 0.0000i$ $-0.7066 + 0.0000i$ $0.0165 + 0.2488i$
	$0.0165 - 0.2488i$ $-0.3263 + 0.0000i$ $-0.2800 + 0.0000i$ $-0.3257 + 0.0000i$ $-0.1260 + 0.0000i$
	$-0.1409 + 0.0000i$ $-0.1507 + 0.0000i$ $-0.1496 + 0.0000i$ $-0.0594 + 0.0000i$ $-0.0693 + 0.0001i$
	$-0.0693 - 0.0001i$ $-0.0274 + 0.0000i$ $-0.0126 + 0.0000i$ $-0.0320 + 0.0000i$ $-0.0320 - 0.0000i$
	$-0.0147 + 0.0000i$ $-0.0147 - 0.0000i$ $0.0000 + 0.0000i$ $0.0000 + 0.0000i$ $0.0000 + 0.0000i$
	$0.0000 + 0.0000i$ $0.0000 + 0.0000i$ $0.0000 + 0.0000i$ $0.0000 + 0.0000i$ $0.0000 + 0.0000i$

**Table 9.** Eigenvalues of the system in presence of biodiesel, GPt, time delay, and RFB (structure-4).

System Condition	Eigenvalue
Hydrothermal system including biodiesel and GPt, time delay, and RFB	-0.1000 + 0.0000i -3.3333 + 0.0000i -0.1000 + 0.0000i -3.3333 + 0.0000i -0.1000 + 0.0000i
	-3.3333 + 0.0000i -0.1000 + 0.0000i -3.3333 + 0.0000i -0.1000 + 0.0000i -3.3333 + 0.0000i
	-12.5000 + 0.0000i -12.5000 + 0.0000i -12.5000 + 0.0000i -12.5000 + 0.0000i -12.5000 + 0.0000i
	-59.9198 + 6.5359i -59.9198 - 6.5359i -56.2001 + 3.4843i -56.2001 - 3.4843i -55.8472 + 7.2876i
	-55.8472 - 7.2876i -49.9874 + 0.0000i -49.9739 + 0.0000i -49.9747 + 0.0000i -36.4359 + 0.0000i
	-35.1881 + 0.0000i -34.7088 + 0.0000i -33.4630 + 0.0000i -33.6403 + 0.0000i -33.7199 + 0.0000i
	-50.0000 + 0.0000i -30.0215 + 0.0000i -28.7628 + 0.0000i -27.9137 + 0.0000i -50.0000 + 0.0000i
	-50.0000 + 0.0000i -16.8387 + 3.1713i -16.8387 - 3.1713i -17.2647 + 0.0000i -15.2569 + 0.0000i
	-15.4193 + 0.0000i -15.4773 + 0.4694i -15.4773 - 0.4694i -13.8376 + 0.0000i -13.6473 + 0.0000i
	-8.3891 + 6.2010i -8.3891 - 6.2010i -12.4523 + 0.0000i -13.1265 + 0.0000i -7.9307 + 0.0000i
	-7.5106 + 0.0000i -7.1518 + 0.0000i -7.1170 + 0.0000i -6.8575 + 0.1307i -6.8575 - 0.1307i
	-6.3711 + 0.0000i -5.9147 + 0.0000i -5.5548 + 0.0000i -1.9044 + 2.1300i -1.9044 - 2.1300i
	-0.1910 + 2.1081i -0.1910 - 2.1081i -3.5930 + 0.0000i -3.5387 + 0.0000i -3.2840 + 0.0000i
	-3.2919 + 0.0000i -3.2353 + 0.1174i -3.2353 - 0.1174i -2.9165 + 0.0000i -2.7281 + 0.0111i
	-2.7281 - 0.0111i -2.1935 + 0.0000i -2.0714 + 0.1040i -2.0714 - 0.1040i -1.5607 + 0.5131i
	-1.5607 - 0.5131i -1.1884 + 0.1830i -1.1884 - 0.1830i -1.5489 + 0.0392i -1.5489 - 0.0392i
	-1.4783 + 0.0575i -1.4783 - 0.0575i -1.4719 + 0.0000i -1.4191 + 0.0000i -0.8067 + 0.0561i
	-0.8067 - 0.0561i -0.8258 + 0.0000i -0.6371 + 0.0291i -0.6371 - 0.0291i -0.6895 + 0.0092i
	-0.6895 - 0.0092i -0.6800 + 0.0000i -0.6539 + 0.0000i -0.3959 + 0.0000i -0.3713 + 0.0117i
	-0.3713 - 0.0117i -0.2945 + 0.0065i -0.2945 - 0.0065i -0.3172 + 0.0023i -0.3172 - 0.0023i
	-0.3128 + 0.0125i -0.3128 - 0.0125i -0.0664 + 0.1304i -0.0664 - 0.1304i -0.2095 + 0.0000i
	-0.1856 + 0.0000i -0.1660 + 0.0000i -0.1305 + 0.0000i -0.1492 + 0.0000i -0.1485 + 0.0076i
	-0.1485 - 0.0076i -0.1460 + 0.0066i -0.1460 - 0.0066i -0.1035 + 0.0000i -0.1124 + 0.0000i
	-0.0526 + 0.0000i -0.0552 + 0.0000i -0.0598 + 0.0000i -0.0717 + 0.0006i -0.0717 - 0.0006i
	-0.0693 + 0.0029i -0.0693 - 0.0029i -0.0698 + 0.0030i -0.0698 - 0.0030i -0.0250 + 0.0000i
	-0.0278 + 0.0000i -0.0332 + 0.0006i -0.0332 - 0.0006i -0.0323 + 0.0010i -0.0323 - 0.0010i
	-0.0114 + 0.0000i -0.0129 + 0.0000i -0.0261 + 0.0000i -0.0157 + 0.0000i -0.0000 + 0.0000i
	-0.0325 + 0.0011i -0.0325 - 0.0011i -0.0121 + 0.0000i -0.0150 + 0.0004i -0.0150 - 0.0004i
	-0.0152 + 0.0000i -0.0151 + 0.0004i -0.0151 - 0.0004i -0.0000 + 0.0000i -0.0000 + 0.0000i
	-0.0000 + 0.0000i -0.0000 + 0.0000i -0.0000 + 0.0000i

**Table 10.** Value of the damping ratio for different conditions of the system using the TIDN-FOID controller.

System Condition	Damping Ratio ( $\xi$ )
Hydrothermal system excluding biodiesel and GPt, time delay, and RFB	0.0085
Hydrothermal system including biodiesel and GPt, time delay, and RFB	0.0903

*Bold signifies best values.*

*5.8. Sensitivity Assessment for a Higher Value of Disturbance*

An examination of sensitivity is performed to detect the robustness of the SHO-augmented TIDN-FOID subordinate controller attributes, focusing on the core characteristics and wide-ranging amendments of the scheme circumstances in T-T-Bd in arena-1, T-T-GPpT in arena-2, and T-H in arena-3 scheme, as well as with RFB and time delay. The inspected scheme was unveiled with 3% step load agitation in arena-1. The optimized attributes of the TIDN-FOID controller shown in Table 11 were obtained by engaging SHO. The results for the premium values similar to basic and wide-ranging outcomes are shown in Figure 10. The outcomes are somewhat comparable, which shows that there is no supplementary rearranging of unsurpassed values when circumstances are altered.

**Table 11.** Related attributes of TIDN-FOID subordinate controllers for structure-4 (i.e., including biodiesel, GPPT, time delay ( $\tau_d$ ), and RFB) at 3% step load disturbance.

Name of Controller	Corresponding Gains and Parameters	Area-1	Area-2	Area-3
TIDN-FOID	$K_{Pi}^*$	0.7016	0.6892	0.6895
	$K_{Ii}^*$	0.6985	0.7985	0.8789
	$K_{Di}^*$	0.4016	0.5014	0.6014
	$N_i^*$	62.25	61.28	62.36
	$n_i^*$	2.1111	2.1875	2.8955
	$K_{FII}^*$	0.8111	0.7895	0.7884
	$\lambda_i^*$	0.0216	0.0356	0.0389
	$K_{FDi}^*$	0.7896	0.7989	0.7954
	$\mu_i^*$	0.1589	0.1586	0.2478

\* Signify the optimum values.

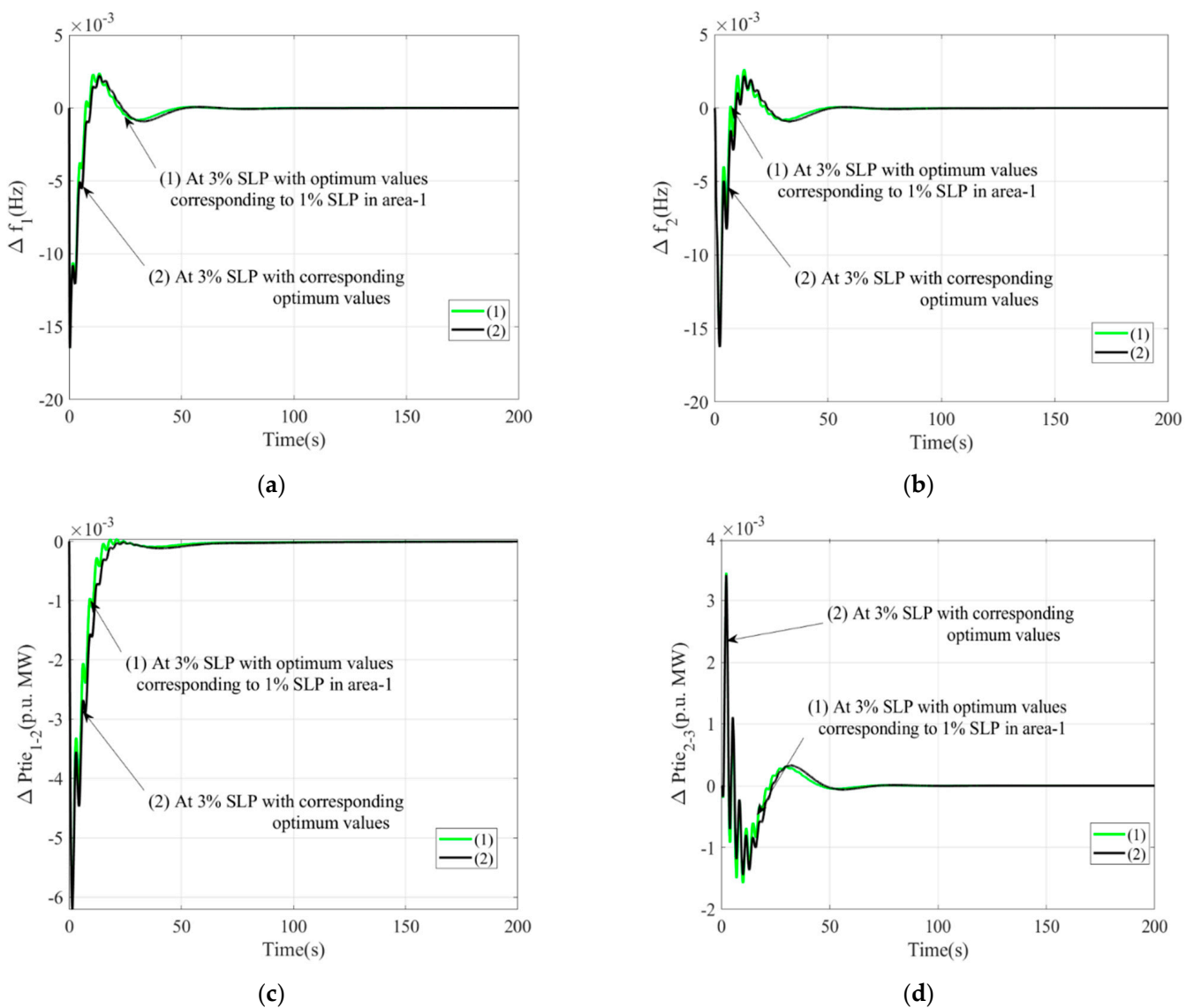


**Figure 10.** Estimation of structure-4 outcomes utilizing the SHO-augmented TIDN-FOID subordinate controller when step load disturbance is increased to 3% from 1% (system with biodiesel, GPPT, time delay, and RFB): (a) arena-1 frequency anomaly, (b) arena-2 frequency anomaly, (c) anomaly in power interrelating arena-1 and -2, and (d) anomaly in power interrelating arena-2 and -3.

## 6. Discussion

According to the results acquired in the preceding subsections, the remarks are as follows:

- (a) The proposed TIDN-FOID controller provides the best results compared to PIDN and TIDN for structure-1, including thermal-thermal-biodiesel energy in area-1, thermal-thermal-GPPt energy in area-2, and hydrothermal energy in area-3. The results in Figure 4 show the superiority of TIDN-FOID compared to PIDN/TIDN, concerning the diminished level of peak overshoot ( $\Delta f_1 = 0.0004$  Hz,  $\Delta f_2 = 0.0003$  Hz,  $\Delta Ptie_{2-3} = 0.0021$  p.u. MW,  $\Delta Ptie_{1-3} = 0.0004$  p.u. MW), extent of oscillations, peak undershoot ( $\Delta f_1 = 0.0153$  Hz,  $\Delta f_2 = 0.0093$  Hz,  $\Delta Ptie_{2-3} = 0.0004$  p.u. MW,  $\Delta Ptie_{1-3} = 0.0042$  p.u. MW), and settling time ( $\Delta f_1 = 62.36$  s,  $\Delta f_2 = 57.44$  s,  $\Delta Ptie_{2-3} = 57.37$  s,  $\Delta Ptie_{1-3} = 56.69$  s).
- (b) The results in Figure 5 show the superiority of system dynamics, using performance index ISE, compared to IAE/ITAE/ITSE, concerning the diminished level of peak overshoot ( $\Delta f_1 = 0.0004$  Hz,  $\Delta Ptie_{2-3} = 0.0021$  p.u. MW,  $\Delta Ptie_{1-3} = 0.0004$  p.u. MW), extent of oscillations, peak undershoot ( $\Delta f_1 = 0.0153$  Hz,  $\Delta Ptie_{2-3} = 0.0004$  p.u. MW,  $\Delta Ptie_{1-3} = 0.0042$  p.u. MW), and settling time ( $\Delta f_1 = 62.36$  s,  $\Delta Ptie_{2-3} = 57.37$  s,  $\Delta Ptie_{1-3} = 56.69$  s).
- (c) In Figure 6, it is observed that the SHO-augmented TIDN-FOID controller provides the lowest value of  $PIx_{ISE}$ , i.e., 0.00071;  $PIx_{ISE}$  values for WOA, PSO, CS, and FA are 0.00077, 0.00078, 0.00081, and 0.00083, respectively. Additionally, SHO provides the lowest computational time value.
- (d) In Figure 7, responses of the systems with and without biodiesel and GPPt are compared. The results in Figure 7 show the superiority of the system with biodiesel and GPP, concerning the diminished level of peak overshoot ( $\Delta f_2 = 0$  Hz,  $\Delta f_3 = 0$  Hz,  $\Delta Ptie_{1-2} = 0$  p.u. MW,  $\Delta Ptie_{1-3} = 0$  p.u. MW), extent of oscillations, peak undershoot ( $\Delta f_2 = 0.009$  Hz,  $\Delta f_3 = 0.0012$  Hz,  $\Delta Ptie_{1-2} = 0.0042$  p.u. MW,  $\Delta Ptie_{1-3} = 0.0041$  p.u. MW), and settling time ( $\Delta f_2 = 52.11$  s,  $\Delta f_3 = 53.42$  s,  $\Delta Ptie_{1-2} = 53.81$  s,  $\Delta Ptie_{1-3} = 53.22$  s).
- (e) In Figure 8, it is shown that the incorporation of time delay degrades the system. However, in order to make the system reflect real-world conditions, an association of time delay is needed; hence, the rest of the assessments were performed with time delay. With time delay, the level of peak overshoot ( $\Delta f_1 = 0.0005$  Hz,  $\Delta f_2 = 0.00046$  Hz,  $\Delta Ptie_{1-2} = 0.0018$  p.u. MW,  $\Delta Ptie_{1-3} = 0.0011$  p.u. MW), peak undershoot ( $\Delta f_1 = 0.015$  Hz,  $\Delta f_2 = 0.011$  Hz,  $\Delta Ptie_{1-2} = 0.0043$  p.u. MW,  $\Delta Ptie_{1-3} = 0.0045$  p.u. MW), and settling time ( $\Delta f_1 = 68.11$  s,  $\Delta f_2 = 67.72$ ,  $\Delta Ptie_{1-2} = 63.42$  s,  $\Delta Ptie_{1-3} = 54.56$  s) were much increased.
- (f) In Figure 9, it is shown that the system with RFB with time delay has a great impact in terms of the diminished level of peak overshoot ( $\Delta f_1 = 0.00001$  Hz,  $\Delta f_3 = 0.00001$  Hz,  $\Delta Ptie_{1-2} = 0$  p.u. MW,  $\Delta Ptie_{1-3} = 0.000001$  p.u. MW), extent of oscillations, peak undershoot ( $\Delta f_1 = 0.0141$  Hz,  $\Delta f_3 = 0.0061$  Hz,  $\Delta Ptie_{1-2} = 0.0021$  p.u. MW,  $\Delta Ptie_{1-3} = 0.0019$  p.u. MW), and settling time overshoot ( $\Delta f_1 = 50.11$  s,  $\Delta f_3 = 50.21$  s,  $\Delta Ptie_{1-2} = 49.81$  s,  $\Delta Ptie_{1-2} = 51.42$  s).
- (g) Eigenvalue assessment was performed to comment on the stability of the system. It is observed that the systems with renewable sources, time delay, and RFB are stable, as they all have eigenvalues with negative real parts and the highest damping ratio.
- (h) In Figure 10, the sensitivity assessment shows that the controllers gains and parameters obtained at the nominal condition for 1% SLP is healthy enough. The values with 1% SLP provide similar responses to those obtained with optimized controller gains and parameters obtained at 3% SLP. Thus, the values should be altered.

## 7. Conclusions

In the current work, biodiesel, along with GPPt, has been unified foremost in the arena of AGC under old-style circumstances. The collective accomplishment of biodiesel and GPP in the contemplated scheme (hydrothermal) offers diminished level of anomalies in peak values ( $C_O$  and  $C_U$ ) and duration of settling ( $S_D$ ). A unique structure has been determined for a dual-step controller with the unification of TIDN and FOID in AGC. A recent, well-known biologically enhanced meta-heuristic procedure expressed as SHO

is competently used to analyze the attributes of varied controllers. The dominance of TIDN-FOID is perceived over extra controllers, such as the proportional-integral-derivative controller with filter and TIDN. The numerical values of  $C_O$ ,  $C_U$ , and  $S_D$  with the proposed cascade TIDN-FOID for  $\Delta f_1$  are 0.0004, 0.0010, and 62.36 s, respectively, whereas the values of PIDN and TIDN are 0.0008, 0.0176, and 118.10 s and 0.0006, 0.0161, and 98.72 s, respectively. Similarly, for other responses, the proposed cascade TIDN-FOID has also shown a significant improvement in  $C_O$ ,  $C_U$ , and  $S_D$ . The impact of non-linearity in the form of time delay was assessed. Even the impact of redox flow battery was analyzed using the TIDN-FOID controller for the system with biodiesel and GPP with time delay. With RFB integration, the standards of  $\Delta f_1$  with  $C_O$ ,  $C_U$ , and  $S_D$  have shown improvements from 0.0005 to 0.00001, 0.015 to 0.014, and 68 s to 50 s, respectively. Furthermore, eigenvalue assessment was performed to judge the systems' stability. The toughness of TIDN-FOID subordinate controller was evaluated by inspecting it with a higher step load value, which shows that the values attained for TIDN-FOID attributes are sufficiently acceptable, and the varying step load disturbance does not need to be altered. The proposed method of frequency control can be applied in the combined control of voltage and frequency in the future. Moreover, it can be applied with a combination of other artificial intelligence techniques.

**Author Contributions:** Conceptualization, N.R.B.; methodology, A.S.; optimization software, L.K.; validation, T.C.; formal analysis, P.D.; investigation, T.C.; resources, M.D.; data curation, N.R.B.; writing—original draft preparation, T.C.; writing—review and editing, N.R.B.; visualization, L.K.; supervision, A.S.; adaptation of optimization procedure, P.D. All authors have read and agreed to the published version of the manuscript.

**Funding:** The research on optimization procedures is supported by the Polish Government, grant number [0212/SBAD/00572].

**Institutional Review Board Statement:** Not applicable.

**Informed Consent Statement:** Not applicable.

**Data Availability Statement:** Not applicable.

**Conflicts of Interest:** The authors declare no conflict of interest.

## Appendix A

- i. Nominal scheme parameters:  $f = 60$  Hz,  $T_{jk,AC} = 0.086$  pu MW/rad,  $H_j = 5$  s,  $K_{pj} = 120$  Hz/MW pu,  $D_j = 8.33 \times 10^{-3}$  pu MW/Hz,  $B_j = 0.425$  pu MW/Hz,  $R_j = 2.4$  pu MW/Hz.
- ii. Thermal component:  $Trk = 10$  s,  $Krk = 5$ ,  $Ttk = 0.3$  s,  $Tgk = 0.08$  s.
- iii. RFB:  $K_r = 1$ ,  $T_d = 0$ ,  $T_r = 0.78$  s,  $K_{RFB} = 1.8$ .
- iv. Hydro:  $T_{RH} = 48.7$  s,  $T_{R1} = 5$  s,  $T_{GH1} = 0.513$  s,  $T_{w1} = 1$  s.
- v. Biodiesel component:  $Kvr_k = 1$ ,  $Tvr_k = 0.05$  s,  $Kce_k = 1$ ,  $Tce_k = 0.5$  s.

## References

1. Elgerd, O.I. *Electric Energy Systems Theory: An Introduction*; Tata McGraw-Hill: New Delhi, India, 2007.
2. Kundur, P. *Power System Stability and Control*; Mc Graw Hill: New Delhi, India, 1993.
3. Ibraheem Kumar, P.; Kothari, D.P. Recent philosophies of automatic generation control strategies in power systems. *IEEE Trans. Power Syst.* **2005**, *20*, 346–357. [[CrossRef](#)]
4. Elgerd, O.I.; Fosha, C.E. Optimum Megawatt-Frequency Control of Multiarea Electric Energy Systems. *IEEE Trans. Power Appar. Syst.* **1970**, *89*, 556–563. [[CrossRef](#)]
5. Das, D.; Aditya, S.K.; Kothari, D.P. Dynamics of diesel and wind turbine generators on an isolated power system. *Electr. Power Energy Syst.* **1999**, *21*, 183–189. [[CrossRef](#)]
6. Das, D.C.; Roy, A.K.; Sinha, N. GA based frequency controller for solar thermal–diesel–wind hybrid energy generation/energy storage system. *Int. J. Electr. Power Energy Syst.* **2012**, *43*, 262–279. [[CrossRef](#)]

7. Ismayil, C.; Sreerama, K.R.; Sindhu, T.K. Automatic generation control of single area thermal power system with fractional order PID (PIAD $\mu$ ) controllers. In Proceedings of the Third International Conference on Advances in Control and Optimization of Dynamical Systems, Kanpur, India, 13–15 March 2014; pp. 552–557.
8. Bhatt, P.; Roy, R.; Ghoshal, S.P. GA/particle swarm intelligence based optimization of two specific varieties of controller devices applied to two-area multi-units automatic generation control. *Int. J. Electr. Power Energy Syst.* **2010**, *32*, 299–310. [[CrossRef](#)]
9. Nanda, J.; Saikia, L.C. Comparison of performances of several types of classical controller in automatic generation control for an interconnected multi-area thermal system. In Proceedings of the 2008 Australasian Universities Power Engineering Conference, AUPEC '08, Sydney, NSW, Australia, 14–17 December 2008.
10. Nanda, J.; Mishra, S.; Saikia, L.C. Maiden application of bacterial foraging based optimization technique in multi area automatic generation control. *IEEE Trans. Power Syst.* **2009**, *24*, 602–609. [[CrossRef](#)]
11. Golpira, H.; Bevrani, H.; Golpira, H. Application of GA optimization for automatic generation control design in an interconnected power system. *Energy Convers. Manag.* **2011**, *52*, 2247–2255. [[CrossRef](#)]
12. Dhamanda, A.; Dutt, A.; Bhardwaj, A.K. Automatic Generation Control in Four Area Interconnected Power System of Thermal Generating Unit through Evolutionary Technique. *Int. J. Electr. Eng. Inform.* **2015**, *7*, 569–583.
13. Saikia, L.C.; Nanda, J.; Mishra, S. Performance comparison of several classical controllers in AGC for multi-area interconnected thermal system. *Int. J. Electr. Power Energy Syst.* **2011**, *33*, 394–401. [[CrossRef](#)]
14. Nanda, J.; Mangla, A.; Suri, S. Some new findings on automatic generation control of an interconnected hydrothermal system with conventional controllers. *IEEE Trans. Energy Convers.* **2006**, *21*, 187–194. [[CrossRef](#)]
15. Abraham, R.J.; Das, D.; Patra, A. AGC of a hydrothermal system with thyristor controlled phase shifter in the tie-line. In Proceedings of the 2006 IEEE Power India Conference, New Delhi, India, 10–12 April 2006.
16. Arya, Y. AGC performance enrichment of multi-source hydrothermal gas power systems using new optimized FOPID controller and redox flow batteries. *Energy* **2017**, *127*, 704–715. [[CrossRef](#)]
17. Panwar, A.; Agarwal, V.; Sharma, G.; Sharma, S. Design of a Novel AGC Action for a Linked Hydro Governing System. *Electr. Power Compon. Syst.* **2021**, *49*, 1201–1211. [[CrossRef](#)]
18. Arya, Y.; Dahiya, P.; Çelik, E.; Sharma, G.; Gözde, H.; Nasiruddin, I. AGC performance amelioration in multi-area interconnected thermal and thermal-hydro-gas power systems using a novel controller. *Eng. Sci. Technol. Int. J.* **2021**, *24*, 384–396. [[CrossRef](#)]
19. Saha, A.; Saikia, L.C. Renewable energy source-based multiarea AGC system with integration of EV utilizing cascade controller considering time delay. *Int. Trans. Electr. Energy Syst.* **2019**, *29*, e2646. [[CrossRef](#)]
20. Tasnin, W.; Saikia, L.C. Performance comparison of several energy storage devices in deregulated AGC of a multi-area system incorporating geothermal power plant. *IET Renew. Power Gener.* **2018**, *12*, 761–772. [[CrossRef](#)]
21. Sharma, G.; Krishnan, N.; Arya, Y.; Panwar, A. Impact of ultracapacitor and redox flow battery with JAYA optimization for frequency stabilization in linked photovoltaic-thermal system. *Int. Trans. Electr. Energy Syst.* **2021**, *31*, e12883. [[CrossRef](#)]
22. Barik, A.K.; Das, D.C. Expedient frequency control of solar photobiotic/biogas/biodiesel generator based isolated renewable microgrid using Grasshopper Optimisation Algorithm. *IET Renew. Power Gener.* **2018**, *12*, 1659–1667. [[CrossRef](#)]
23. Gupta, N.; Kumar, N. Particle swarm optimization based automatic generation control of interconnected power system incorporating battery energy. *Procedia Comput. Sci.* **2018**, *132*, 1562–1569. [[CrossRef](#)]
24. Sharma, G.; Narayanan, K.; Adefarati, T.; Sharma, S. Frequency regularization of a linked wind–diesel system using dual structure fuzzy with ultra-capacitor. *Prot. Control Mod. Power Syst.* **2022**, *7*, 1–9. [[CrossRef](#)]
25. Arya, Y. Effect of energy storage systems on automatic generation control of interconnected traditional and re-structured energy systems. *Int. J. Energy Res.* **2019**, *43*, 6475–6493. [[CrossRef](#)]
26. Pathak, N.; Verma, A.; Bhatti, T.S.; Nasiruddin, I. Modeling of HVDC tie-links and their utilization in AGC/LFC operations of multi-area power systems. *IEEE Trans. Ind. Electron.* **2019**, *66*, 2185–2197. [[CrossRef](#)]
27. Kumari, N.; Malik, N.; Jha, A.N.; Malleshm, G. Design of PI Controller for Automatic Generation Control of Multi Area Interconnected Power System using Bacterial Foraging Optimization. *Int. J. Eng. Technol.* **2016**, *8*, 2779–2786. [[CrossRef](#)]
28. Jagatheesan, K.; Anand, B.; Samanta, S.; Dey, N.; Ashour, A.S.; Balas, V.E. Design of a proportional-integral-derivative controller for an automatic generation control of multi-area power thermal systems using firefly algorithm. *IEEE/CAA J. Autom. Sin.* **2019**, *6*, 503–515. [[CrossRef](#)]
29. Dash, P.; Saikia, L.C.; Sinha, N. Comparison of performances of several FACTS devices using Cuckoo search algorithm optimized 2DOF controllers in multi-area AGC. *Electr. Power Energy Syst* **2015**, *65*, 316–324. [[CrossRef](#)]
30. Rahman, A.; Saikia, L.C.; Sinha, N. AGC of dish-stirling solar thermal integrated thermal system with biogeography based optimised three degree of freedom PID controller. *IET Renew. Power Gener.* **2016**, *10*, 1161–1170. [[CrossRef](#)]
31. Reddy, P.J.; Kumar, T.A. AGC of three-area hydro-thermal system in deregulated environment using FOPI and IPFC. In Proceedings of the 2017 International Conference on Energy, Communication, Data Analytics and Soft Computing (ICECDS), Chennai, India, 1–2 August 2017; pp. 2815–2821. [[CrossRef](#)]
32. Dekaraja, B.; Saikia, L.C.; Ramoji, S.K.; Behera, M.K.; Bhagat, S.K. Impact of RFB and HVDC link on Combined ALFC-AVR Studies of a GTPP Integrated Hydro-thermal Systems Using a Cascade Fuzzy PD-TID Controller. In Proceedings of the 2022 4th International Conference on Energy, Power and Environment (ICEPE), Shillong, India, 29 April–1 May 2022. [[CrossRef](#)]
33. Pan, I.; Das, S. Fractional order AGC for distributed energy resources using robust optimization. *IEEE Trans. Smart Grid* **2016**, *7*, 2175–2186. [[CrossRef](#)]



34. Ismayil, C.; Sreerama, R.K.; Sindhu, T.K. Fractional order pid controller for automatic generation control of multiarea power systems. *Int. Trans. Electr. Energy Syst.* **2015**, *25*, 3329–3348. [[CrossRef](#)]
35. Ramoji, S.K.; Saikia, L.C.; Dekaraja, B.; Behera, M.K.; Bhagat, S.K. Performance Comparison of Various Tilt Controllers in Coalesced Voltage and Frequency Regulation of Multi-Area Multi-Unit Power System. In Proceedings of the 2022 IEEE Delhi Section Conference (DELCON), New Delhi, India, 11–13 February 2022. [[CrossRef](#)]
36. Rajput, G.K.; Yadav, A.; Kumar, A.; Gautam, A.; Tiwari, A.; Babu, N.R.; Chiranjeevi, T. Design of TID controller based on firefly algorithm for controlling the speed of a DC Motor. *E3S Web Conf.* **2020**, *184*, 01038. [[CrossRef](#)]
37. Moschos, I.; Parisses, C. A novel optimal  $PI^{\lambda}DND^2N^2$  controller using coyote optimization algorithm for an AVR system. *Eng. Sci. Technol. Int. J.* **2022**, *26*, 100991. [[CrossRef](#)]
38. Sharma, P.; Prakash, A.; Shankar, R.; Parida, S.K. A Novel Hybrid Salp Swarm Differential Evolution Algorithm Based 2DOF Tilted-Integral-Derivative Controller for Restructured AGC. *Electr. Power Compon. Syst.* **2019**, *47*, 1775–1790. [[CrossRef](#)]
39. Abd-Elazim, S.M.; Ali, E.S. Load frequency controller design via BAT algorithm for nonlinear interconnected power system. *Int. J. Electr. Power Energy Syst.* **2016**, *77*, 166–177. [[CrossRef](#)]
40. Arya, Y.; Kumar, N.; Dahiya, P.; Sharma, G.; Çelik, E.; Dhundhara, S.; Sharma, M. Cascade- $\lambda$ AD $\mu$ N controller design for AGC of thermal and hydro-thermal power systems integrated with renewable energy sources. *IET Renew Power Gener.* **2021**, *15*, 504–520. [[CrossRef](#)]
41. Sharma, G.; Panwar, A.; Arya, Y.; Kumawat, M. Integrating layered recurrent ANN with robust control strategy for diverse operating conditions of AGC of the power system. *IET Gener. Transm. Distrib.* **2020**, *14*, 3886–3895. [[CrossRef](#)]
42. Sharma, M.; Dhundhara, S.; Arya, Y.; Prakash, S. Frequency stabilization in deregulated energy system using coordinated operation of fuzzy controller and redox flow battery. *Int J Energy Res.* **2021**, *45*, 7457–7475. [[CrossRef](#)]
43. Venkateswara Rao, B.; Devarapalli, R.; Malik, H.; Bali, S.K.; García Márquez, F.P.; Chiranjeevi, T. Wind integrated power system to reduce emission: An application of bat algorithm. *J. Intell. Fuzzy Syst.* **2022**, *42*, 1041–1049. [[CrossRef](#)]
44. Vandrasi, R.K.; Kumar, B.S.; Devarapalli, R. Solar photo voltaic module parameter extraction using a novel Hybrid Chimp-Sine Cosine Algorithm. *Energy Sources Part A Recovery Util. Environ. Eff.* **2022**. [[CrossRef](#)]
45. Devarapalli, R.; Kumar, V. Power system oscillation damping controller design: A novel approach of integrated HHO-PSO algorithm. *Arch. Control Sci.* **2021**, *31*, 553–591.
46. Devarapalli, R.; Sinha, N.K.; García Márquez, F.P. A review on the computational methods of power system stabilizer for damping power network oscillations. *Arch. Comput. Methods Eng.* **2022**, *29*, 3713–3739. [[CrossRef](#)]
47. Verma, S.K.; Devarapalli, R. Fractional order  $PIAD\mu$  controller with optimal parameters using Modified Grey Wolf Optimizer for AVR system. *Arch. Control Sci.* **2022**, *32*, 429–450.
48. Ram Babu, N.; Bhagat, S.K.; Saikia, L.C.; Chiranjeevi, T.; Devarapalli, R.; García Márquez, F.P. A Comprehensive Review of Recent Strategies on Automatic Generation Control/Load Frequency Control in Power Systems. *Arch. Comput. Methods Eng.* **2022**. [[CrossRef](#)]
49. Saha, A.; Dash, P.; Babu, N.R.; Chiranjeevi, T.; Venkateswararao, B.; Knypiński, Ł. Impact of Spotted Hyena Optimized Cascade Controller in Load Frequency Control of Wave-Solar-Double Compensated Capacitive Energy Storage Based Interconnected Power System. *Energies* **2022**, *15*, 6959. [[CrossRef](#)]
50. Devarapalli, R.; Kumar Sinh, N.; Bathinavenkateswara, R.; Knypiński, Ł.; Jaya Naga, N.; Marquez, F.P.G. Allocation of real power generation based on computing over all generation cost: An approach of Salp Swarm Algorithm. *Arch. Electrical. Eng.* **2021**, *70*, 337–349.
51. Knypiński, Ł. Constrained optimization of line-start PM motor based on the grey wolf optimizer. *Eksplot. I Niezawodn.—Maint. Reliab.* **2021**, *23*, 1–10. [[CrossRef](#)]
52. Knypiński, Ł.; Kuroczycki, S.; Márquez, F.P.G. Minimization of Torque Ripple in the Brushless DC Motor Using Constrained Cuckoo Search Algorithm. *Electronics* **2021**, *10*, 2299. [[CrossRef](#)]
53. Madasu, S.D.; Sai Kumar, M.L.S.; Singh, A.K. A flower pollination algorithm based automatic generation control of interconnected power system. *Ain Shams Eng. J.* **2018**, *9*, 1215–1224. [[CrossRef](#)]
54. Sahu, R.K.; Panda, S.; Rout, U.K. DE optimized parallel 2-DOF PID controller for load frequency control of power system with governor dead-band nonlinearity. *Int. J. Elect. Power Energy Syst.* **2013**, *49*, 19–33. [[CrossRef](#)]
55. Panwar, A.; Agarwal, V.; Sharma, G. Studies on Frequency Regulation of Hydro System via New JAYA Optimized LQR Design. In Proceedings of the 2021 International Conference on Artificial Intelligence, Big Data, Computing and Data Communication Systems (icABCD), Durban, South Africa, 5–6 August 2021. [[CrossRef](#)]
56. Dhiman, G.; Kumar, V. Spotted hyena optimizer: A novel bio-inspired based metaheuristic technique for engineering applications. *Adv. Eng. Softw.* **2017**, *114*, 48–70. [[CrossRef](#)]
57. Alghamdi, M.I. Optimization of Load Balancing and Task Scheduling in Cloud Computing Environments Using Artificial Neural Networks-Based Binary Particle Swarm Optimization (BPSO). *Sustainability* **2022**, *14*, 11982. [[CrossRef](#)]
58. Salah, B.; Hasanien, H.M.; Ghali, F.M.A.; Alsayed, Y.M.; Abdel Aleem, S.H.E.; El-Shahat, A. African Vulture Optimization-Based Optimal Control Strategy for Voltage Control of Islanded DC Microgrids. *Sustainability* **2022**, *14*, 11800. [[CrossRef](#)]
59. Dai, L.; Lu, H.; Hua, D.; Liu, X.; Chen, H.; Glowacz, A.; Królczyk, G.; Li, Z. A Novel Production Scheduling Approach Based on Improved Hybrid Genetic Algorithm. *Sustainability* **2022**, *14*, 11747. [[CrossRef](#)]

- 
60. Chiranjeevi, T.; Devarapalli, R.; Babu, N.R.; Vakkapatla, K.B.; Rao, G.S.; Marquez, P.G. Fixed terminal time fractional optimal control problem for discrete time singular system. *Arch. Control Sci.* **2022**, *32*, 489–506.
  61. Oustaloup, A.; Mathieu, B.; Lanusse, P. The CRONE Control of Resonant Plants: Application to a Flexible Transmission. *Eur. J. Control* **1995**, *1*, 113–121. [[CrossRef](#)]